Evaluating Sprinkler Fire Protection for Multiple Row Rack Systems

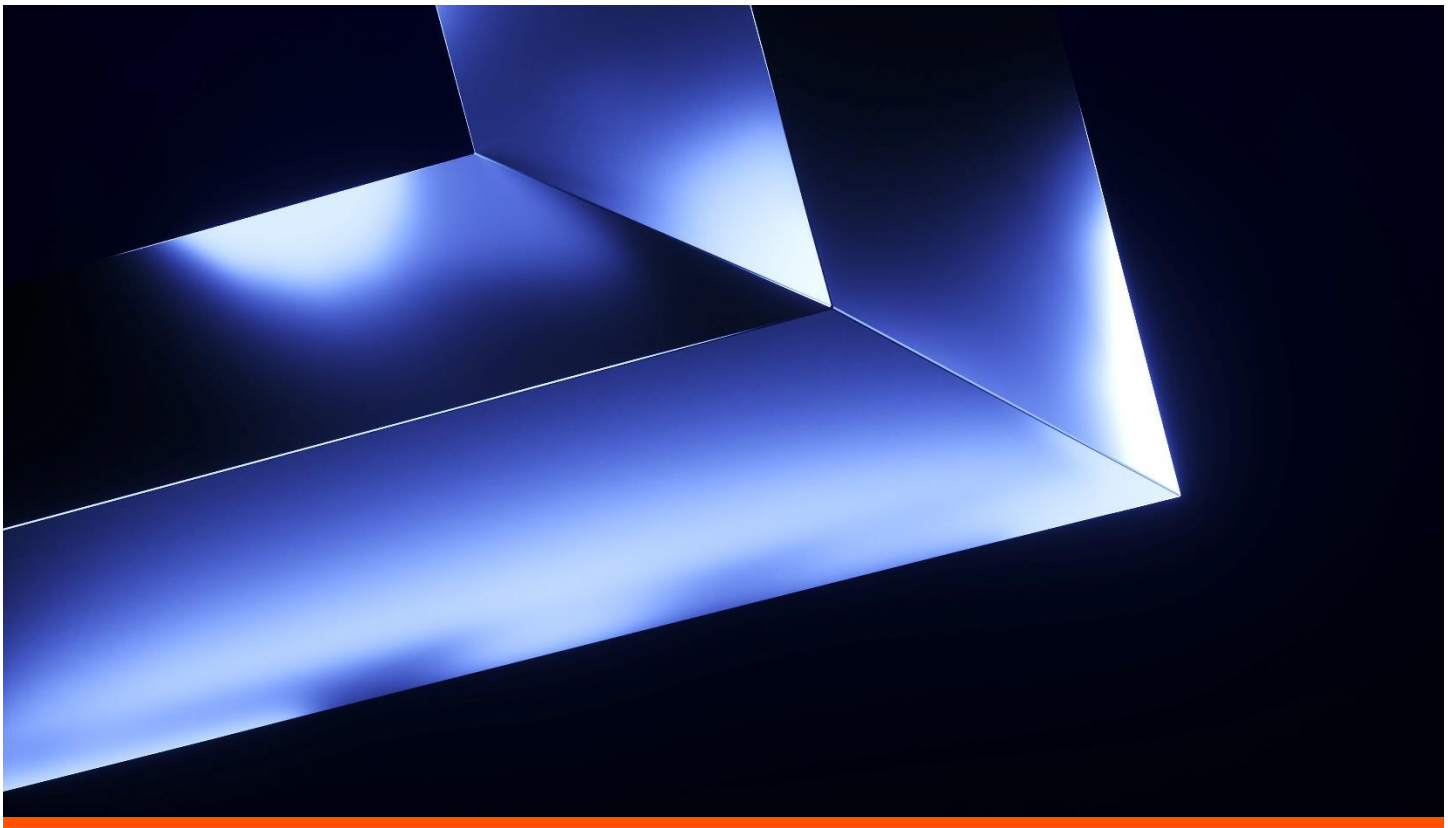

TECHNICAL REPORT

Evaluating Sprinkler Fire Protection for Multiple Row Rack Systems

Prepared by

Dong Han
Ning Ren

FM
One Technology Way, Norwood, MA 02062

May 2026

Project ID: RW000605

Disclaimer

The research presented in this report, including any findings and conclusions, is for informational purposes only. Any references to specific products, manufacturers, or contractors do not constitute a recommendation, evaluation or endorsement by Factory Mutual Insurance Company (FM) of such products, manufacturers or contractors. FM does not address life, safety, or health issues. The recipient of this report must make the decision whether to take any action. FM undertakes no duty to any party by providing this report or performing the activities on which it is based. FM makes no warranty, express or implied, with respect to any product or process referenced in this report. FM assumes no liability by or through the use of any information in this report.

Executive Summary

This report presents a comprehensive evaluation of sprinkler fire protection strategies for multiple row rack (MRR) storage systems, which are increasingly utilized in high-density warehouse environments. MRRs come in many shapes and sizes, most of which are deeper than 6.1 m (20 ft) and do not have longitudinal flues (closed-array storage). The requirements from the latest edition (2025) of NFPA 13 mandate the installation of in-rack sprinklers at every tier for these types of storage racks. Some stakeholders have identified implementation challenges associated with this approach, highlighting the need to further evaluate appropriate protection strategies for MRRs.

This study is part of a multi-phase project conducted in conjunction with the Property Insurance Research Group (PIRG) and in partnership with the Fire Protection Research Foundation (FPRF). The work investigated the effectiveness of current ceiling-only sprinkler protection recommendations and explored alternative solutions for closed-array MRR configurations, through a combination of intermediate-scale and large-scale fire tests, as well as advanced computational fluid dynamics (CFD) modeling. Intermediate-scale experiments were designed to understand the fire hazards of MRR with different parameters, while CFD modeling using FireFOAM also guided the design of large-scale tests beyond the reach of intermediate-scale tests.

Key findings indicate that the seamless cartoned unexpanded plastic (CUP) commodity, defined in this work, should be used as the representative commodity for closed-array MRRs as it poses a greater challenge due to limited water pathways, necessitating higher delivered water density for effective fire control, as compared to the standard CUP commodity. Additional findings also demonstrate that certain MRR features, such as angle irons and slopes, have minimal impact on suppression outcomes. A different worst-case ignition scenario was identified by simulations compared with double-row arrays.

Large-scale test results reveal that existing protection guidance using K240 lpm/bar$^{1/2}$ (16.8 gpm/psi$^{1/2}$) sprinklers at 3.6 bar (52 psi) is inadequate for closed-array MRR storage which is 10.4 m (34 ft) tall and 6.4 m (21 ft) deep under a 12.2 m (40 ft) ceiling, resulting in excessive sprinkler activations and uncontrolled flame spread. Enhanced protection with the same K240 lpm/bar$^{1/2}$ (16.8 gpm/psi$^{1/2}$) sprinklers at an elevated pressure of 6.2 bar (90 psi) or larger K360 lpm/bar$^{1/2}$ (25 gpm/psi$^{1/2}$) sprinklers at 2.8 bar (40 psi) provide adequate protection with more effective fire control and fewer sprinkler activations. The large-scale testing also highlights operational challenges of manual firefighting in MRR environments, emphasizing the need to develop emergency plans owners or operators based on local fire department capabilities with fire service's input and available water supply in the protection design.

Moving forward, the validated CFD models can serve as a practical engineering tool for MRR fire protection development for a wider range of MRR configurations, with different ceiling heights, commodities, and sprinklers. In-rack sprinkler protection was not addressed in this effort but remains an important consideration for retrofit scenarios.

Abstract

The performance of ceiling-only sprinkler protection in closed-array multiple row rack (MRR) storage configurations was investigated through intermediate- and large-scale fire tests and validated numerical modeling. Results demonstrate that seamless cartoned unexpanded plastic (CUP) commodities require higher delivered densities than standard CUP commodities due to reduced water pathways. Rack features such as angle irons and slopes show limited influence on fire control, while ignition location becomes a critical factor in flame spread. Large-scale testing confirmed that current ceiling-only protection options from both NFPA 13 and FM Property Loss Prevention Data Sheets are inadequate for closed-array MRR storage. Adequate protection was achieved using higher water pressure and larger K-factor sprinklers. The findings underscore the importance of final extinguishment in sprinkler designs for MRRs. Final recommendations are provided for both existing and new facilities, addressing operational limitations and future research directions to advance fire protection of MRR systems.

Acknowledgements

The authors thank Mr. Kevin Mullins, Mr. Ryan Foley, and Mr. Jason Tucker of the FM Research Campus for their coordination of the tests conducted in the large burn laboratory. Additional thanks are given to staff at the Research Campus for handling materials and conducting tests. The authors would also like to thank Mr. Brent Wunderlich, Mr. Matthew J. Daelhousen, and Mr. Weston Baker of the Chief Engineer's Group for providing directions and feedback for engineering applications. The authors also want to thank Dr. Sergey Dorofeev, Dr. Yi Wang, Dr. Yibing Xin, Mr. Benjamin Ditch, Dr. James White, and Mr. Seth Sienkiewicz for their invaluable discussions during this work. A special thank you to Ms. Amanda Kimball and Ms. Jacqueline Wilmot from the Fire Protection Research Foundation for facilitating the project and Mr. Tracey Bellamy from Telgian Engineering & Consulting for collaborative efforts on test designs. Finally, the authors would like to thank members of the Fire Protection Research Foundation technical panel and the Property Insurance Research Group for their valuable discussions and interactions during this project.

Table of Contents

List of Figures

List of Tables

1. Introduction

Multiple row rack (MRR) systems are high-density storage solutions engineered to optimize space utilization in warehouses, distribution centers, and manufacturing facilities. By arranging racks in multiple rows and tiers, these systems enable businesses to store a large volume of goods efficiently while maintaining accessibility and organization. They are essential components in modern logistics and supply chain operations, supporting efficient inventory management and quick retrieval of products.

The MRR systems found in modern warehouses come in many shapes and sizes, with different technologies involved. Four common types are briefly introduced here, including gravity-driven systems, shuttle pallet systems, drive-in/drive-through racking systems, and mobile racking systems. This is not meant to be a comprehensive list as there are many other storage systems considered as MRR by definition due to lack of aisles, especially when used for smaller products where 1.2-m (4-ft) aisles (1.1 m [3.5 ft] by NFPA 13, 2025 edition) are needed [1, 2]. Those systems, including many automated storage and retrieval systems (ASRS) with containers/bins and very narrow aisle (VNA) storage systems, are outside the scope of this work and can be investigated in separate studies. The four types of MRR considered in this work are described as follows.

Gravity-driven systems, including flow-through racks and push-back racks, utilize the force of gravity to move items within the rack. Flow-through racks, as shown in Fig. 1-1(a) and also known as first-in-first-out (FIFO) racks, are slightly tilted to allow goods to slide down smoothly on roller rails from the loading end to the picking end. Alternatively, push-back racks use a series of nested carts that move along inclined rails. When a new pallet is loaded, it pushes the previous pallet back, making this system suitable for last-in-first-out (LIFO) storage.

Shuttle pallet systems can be semi-automated or fully automated and employ motorized shuttles to transport pallets within the rack. These shuttles travel along rails and can be controlled remotely, significantly enhancing storage density by eliminating the need for forklift aisles between rack bays. Variants of shuttle systems include 2-way shuttles, as shown in Fig. 1-1(b), 4-way shuttles, and mother-child systems, each offering different levels of maneuverability and functionality.

Drive-in and drive-through racking systems are shown in Fig. 1-1(c), which allow forklifts to enter the rack structure to place and retrieve pallets. Drive-in racking is designed for high-density storage of homogeneous products, while drive-through racking permits access from both ends, facilitating FIFO rotation.

Finally, mobile racking systems are shown in Fig. 1-1(d), which combine high-density storage with direct access to each pallet. These racks are mounted on motorized mobile bases that move laterally along rails, increasing storage capacity by 80-120% compared to conventional pallet racking.

All four system types have minimal presence of aisles, which are needed for traditional single row racks (SRRs) and double row racks (DRRs) to access stored goods, thereby resulting in a more space-efficient use of storage areas. However, they also present challenges demanding stringent fire protection requirements. The 2025 edition of NFPA 13 [2] limits the depth of an MRR system to no more than 6.1 m (20 ft) unless 150 mm (6 in.) longitudinal and transverse flues are provided around each pallet load. Otherwise, in-rack sprinkler protection is needed at every tier of storage, in accordance with the mandated provision for protection of solid-shelf storage.

The basis of the above provisions can be traced back to 1971, where a large-scale test (Test No. 107) was conducted using an MRR of Class II commodity [3]. The storage rack was 4.7 m (16 ft) deep with 150 mm (6 in.) transverse flues between adjacent pallet loads and no longitudinal flue. The fire activated 12 ceiling sprinklers over a duration of 96 minutes and extended to the full depth of the rack, which would presumably spread further had the test array been deeper. A recommendation to limit the storage depth to 4.7 m (16 ft) was introduced based on this test. Another large-scale test, (Test No. 151) in the same program, using a similar but deeper storage array about 8.5 m (28 ft) long was conducted with both ceiling and in-rack sprinkler protection [3]. In this test, three ceiling sprinklers and two in-rack sprinklers operated over a duration of 45 minutes, and the fire was confined within the array. The results of both tests led to the recommendations in the 1980 edition of NFPA 231C for MRRs using control-model, density-area (CMDA) sprinkler protection.

In 1986, the National Fire Protection Research Foundation (NFPRF) sponsored a large-scale test program in conjunction with a required delivered density (RDD) test to evaluate the effectiveness of early suppression fast response (ESFR) sprinklers on

MRR storage arrays [4]. The RDD test was used to examine the relative fire severity of two different storage configurations, namely an open array defined as an array with 15-cm (6-in.) flues in both directions and a closed array defined as an array with 15-cm (6-in.) flues only in one direction. The test consisted of a two-pallet long by two-pallet deep by four-pallet tall array of FM standard cartoned unexpanded plastic (CUP) commodity, placed under a water application apparatus, which delivered a uniform water flux of 20 mm/min (0.5 gpm/ft^2) onto the top surface of the array. A conclusion was made after comparing the convective heat release rate (HRR) curves from both configurations: the closed array posed lower hazard than the open array.

Figure 1-1: Commonly found multiple row racks in modern warehouses: (a) flow-through racks, (b) shuttle pallet systems, (c) drive-through racks, and (d) mobile racks

This conclusion was adopted in the large-scale test program to develop protections applicable to both configurations. The large-scale test was conducted under a 9.1-m (30-ft) ceiling using a 7.3-m (24-ft) high open array. Sprinkler protection was provided from the ceiling only, using the same design scheme for DRR storage, i.e. K200 lpm/bar$^{1/2}$ (K14 gpm/psi$^{1/2}$), 74°C (165°F) rated, quick response, pendent sprinklers operated at 3.4 bar (50 psi). The fire was controlled by four sprinklers, concluding that adequate protection for DRRs can also be applied to MRRs.

There are also other MRR fire tests using varying commodities in both open and closed arrays. Those tests involved non-standard commodities or protection techniques such as barriers, serving a good reference for understanding the MRR fire hazards. A detailed review can be found in Ref. [5].

This report describes part of a multi-phase project conducted in conjunction with the Property Insurance Research Group (PIRG) and in partnership with the Fire Protection Research Foundation (FPRF). The overarching goal of this work was to evaluate existing ceiling-only protection recommendations in both NFPA 13, *Standard for the Installation of Sprinkler Systems* [2], and FM Property Loss Prevention Data Sheet 8-9, *Storage of Class 1, 2, 3, 4 and Plastic Commodities* [1], for MRR systems using closed arrays. To provide a proper evaluation, this work was divided into two phases. Phase 1 focused on understanding the hazard of MRR systems, through intermediate-scale tests and numerical modeling, with the objectives of identifying proper representative configurations for large-scale tests as well as developing and validating numerical models to support the design of adequate sprinkler protections. Phase 2 followed with large-scale tests to evaluate protection designs based on current guidance and observations in existing facilities, and those for new facilities. This report is structured by documenting Phase 1 and 2 in Chapters 2 and 3, respectively, including both the methods and results. The final conclusions and recommendations are provided in Chapter 4.

2. Phase 1: Understanding the Hazards

2.1 Experimental Methods: Intermediate-Scale Tests

Eight intermediate-scale tests were conducted under the 20-MW fire products collector (FPC) in the large burn laboratory (LBL) at the FM Research Campus in West Glocester, RI, USA. Figure 2-1 shows the test setup using the water application apparatus (WAA). The WAA includes 48 full-cone spray nozzles installed on six suppression pipes on 0.6 m × 0.6 m (2 ft × 2 ft) spacing positioned 20 cm (8 in.) above the top of the fuel array. The nozzles, manufactured by Spraying Systems Co., were used to provide a uniform water flux toward the top of the fuel array. The spray nozzles were activated based on the response of a virtual sprinkler thermal element placed 3.05 m (10 ft) above the fuel array, with an activation temperature of 141°C (286°F) and a response time index of 276 $(m \cdot s)^{1/2}$ [500 $(ft \cdot s)^{1/2}$]. The link temperature of this virtual sprinkler was calculated during the tests using the calorimeter-measured HRR data and ceiling flow correlations [6]. More details about the WAA can be found in Ref. [7].

The fuel array, shown in Fig. 2-2, consisted of a five-tier MRR storage with three rows, four-pallet deep, measuring 3.5 m (11.5 ft) wide, 4.3 m (14 ft) deep, and 7.3 m (24 ft) tall. The rows were separated by a 15-cm (6-in.) flue. Within each row, commodities were butted together (without flues). This array design was used in all tests except Tests 6 and 7, where special features were introduced. In Test 6, angle irons, shown in Fig. 2-3, were installed on every tier along each row, directly beneath the commodity, representing a critical feature seen in drive-in/through MRR systems. The angle irons were in an L-shape, measuring 5 cm (2 in.) by 5 cm (2 in.). They were installed such that a 2.5 cm (1 in.) gap was maintained between the commodity and the vertical bar of an angle iron as shown in Fig. 2-3, which could create a channel to direct sprinkler water to the aisle, potentially reducing the effectiveness of ceiling sprinkler protection.

Slopes were introduced in Test 7 to simulate a gravity-driven MRR system, as shown in Fig. 2-4. The implementation of a slope of 4 degrees represents a maximum slope based on feedback from MRR manufacturers. The purpose was to understand the impact of slope on ceiling sprinkler protection, which could direct water to one side of the array, creating under-protected or dry spots on the other side of the array.

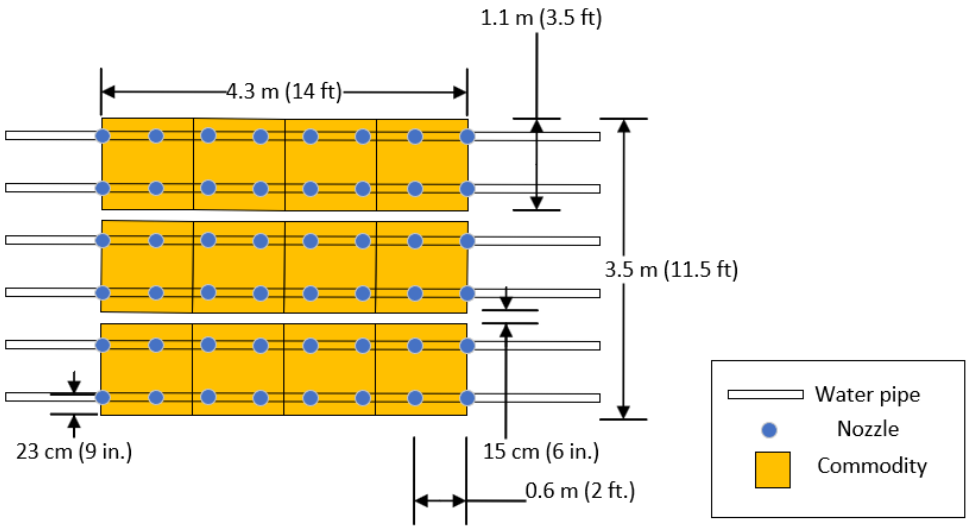

Figure 2-1: Plan-view schematic of the intermediate-scale test setup

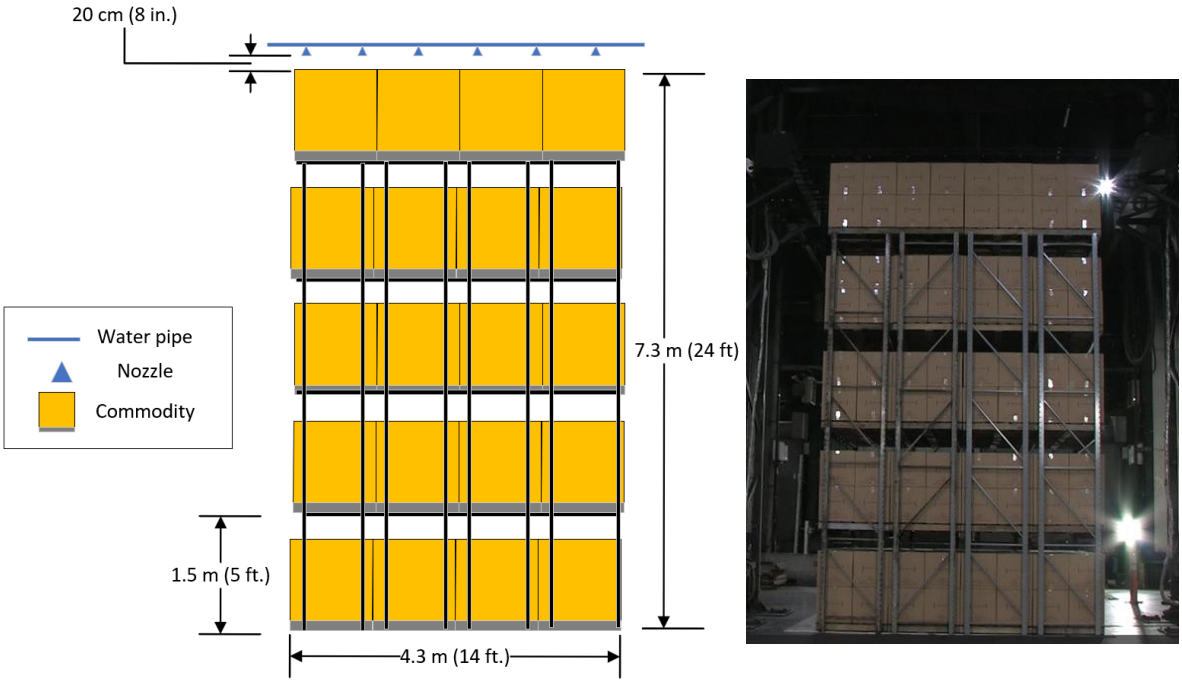

Figure 2-2: Elevation-view schematic (left) and image (right) of the intermediate-scale test setup

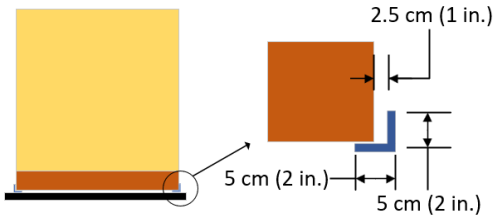

Figure 2-3: Schematic showing angle irons added to the rack structure for Tests 6 and 7

The Phase 1 study considered two commodities, including the FM standard CUP commodity and a modified 'seamless' CUP commodity. The latter represents commodities that provide no water transport pathways within the pallet load (such as Gaylord boxes or other fully encapsulated pallet loads). Images of each CUP type are shown in Fig. 2-5. The seamless CUP commodity was made by placing one single-wall cardboard sheet on the top and bottom of the boxes, secured with staples. Both CUP types would be treated the same in NFPA 13 as Group A plastic commodity for open arrays. However, for closed arrays, it was concerned that the seamless CUP type may perform worse than standard CUP. The main effect of the seams is to reduce dry spots persisting on top of boxes that are not on top tier. This would make seamless CUP suppression more difficult in all cases, but particularly significant in MRR as it can lead to an uninterrupted dry surface for the fire to spread along. Note that there are still seams between the pallet loads to allow some water to seep through.

Two ignition locations were used, as shown in Fig. 2-6. Both ignition locations were offset from the center of the array by one pallet load to provide as much space as possible for lateral flame spread in one direction before reaching the end of the array. The ignitors were placed either along the flue on the floor (i.e., flue ignition) or on top of the first tier along the center of the array (i.e., top ignition). The top ignition scenario was investigated to determine if it was worse than the flue ignition scenario for MRR systems. The primary concern for the top ignition scenario was that it may delay vertical flame spread in flue spaces while promoting lateral spread along the row, which could result in a larger fire before the first sprinkler activation and potentially more sprinkler activations. Four standard half ignitors were used in both scenarios, evenly placed around the center of ignition mark as red squares shown in the zoomed-in views in Fig. 2-6. The standard half ignitors were made of

cotton cellulose material wrapped in cheesecloth, each 7.6 cm (3 in.) in diameter and 7.6 cm (3 in.) long. Each ignitor was soaked with 120 mL (4 oz.) of gasoline and sealed in a clear plastic bag. A propane torch was used to ignite the ignitors, signaling the onset of each test.

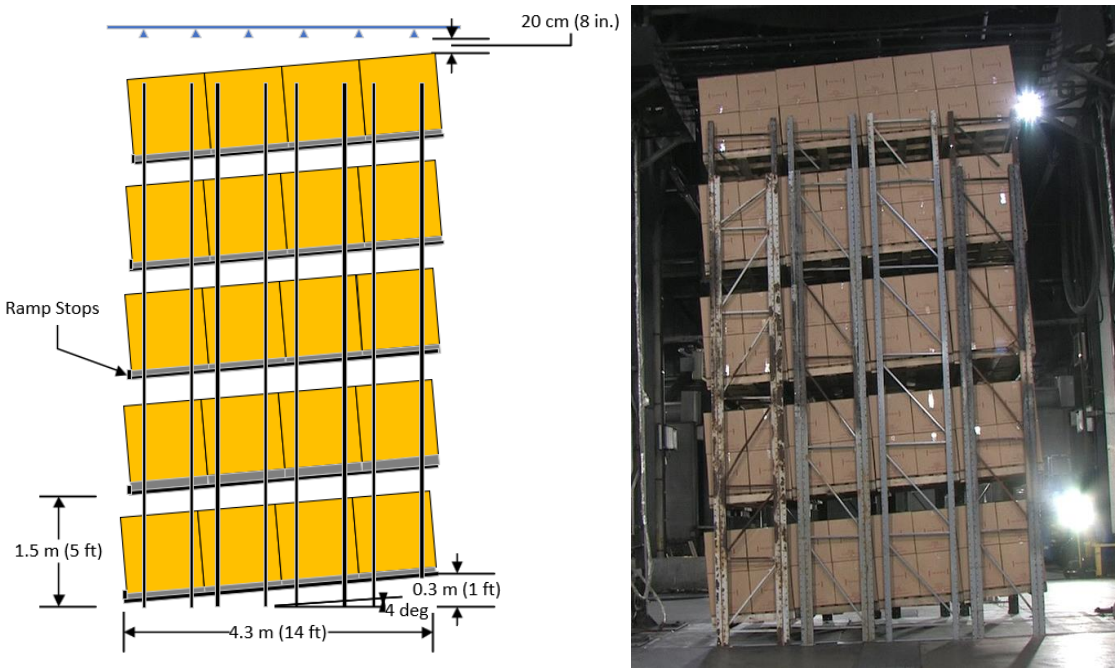

Figure 2-4: Elevation-view schematic (left) and image (right) of the intermediate-scale test setup with slope

Figure 2-5: Images of standard CUP (left) and seamless CUP (right) commodities

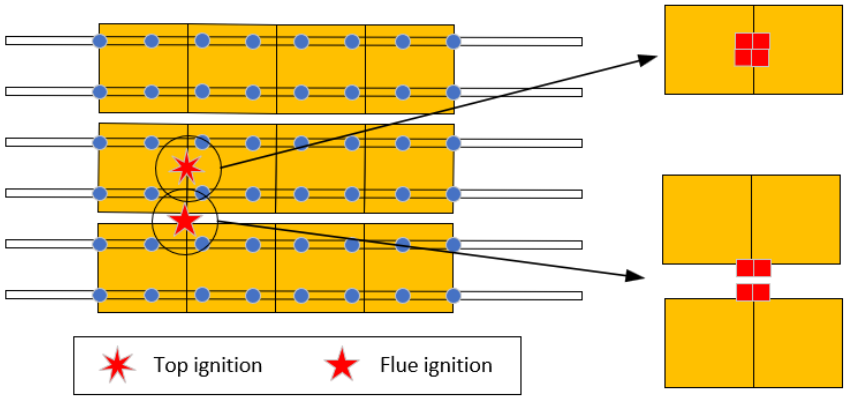

Figure 2-6: Schematic of top and flue ignition locations

The tests were recorded using both visible and infrared (IR) video cameras and still photographs. Bullet cameras were inserted into the storage array on the second and fourth tiers to monitor water transport processes such as transport time and the influence of the angle irons. Figure 2-7 shows the camera positions.

Table 2-1 lists the test matrix of Phase 1. Note that "IS" in the test number stands for intermediate scale. Tests IS-1 and IS-2 investigated the influence of water transport between seams within commodities by comparing standard CUP (Test IS-1) and seamless CUP (Test IS-2). To better highlight the influence, the water density was selected close to the marginal condition so that the fire suppression performance would be more sensitive to the difference in test configuration. A density of 24 mm/min (0.6 gpm/ft^2) was selected, which was slightly higher than the critical delivered flux (CDF) for standard CUP in a 5-tier open array [8]. The worst-performing CUP type (seamless CUP) was then used to study the influences of ignition location, presence of angle irons, and presence of slope in Tests IS-5 through IS-7, respectively. Before those tests, two additional water densities were evaluated in Tests IS-3 and IS-4 to determine the appropriate value for Tests IS-5 through IS-7, with a target slightly greater than the CDF of seamless CUP with flue ignition. One more test (Test IS-8) was conducted to evaluate the CDF for seamless CUP with top ignition. During this test series, different nozzles were used according to the water densities to ensure a consistent mean droplet diameter of 1.75±0.35 mm (0.069±0.014 in.) in the water spray.

The results of tests were evaluated using chemical HRR data measured by the calorimeter, extent of flame spread, and observations of critical phenomena related to fire suppression. Note that the test outcomes were not evaluated for pass or failure. Instead, they served as parametric studies to help understand the impact of different parameters, and to provide validation cases for numerical models, as well as to support the development of representative large-scale test configurations.

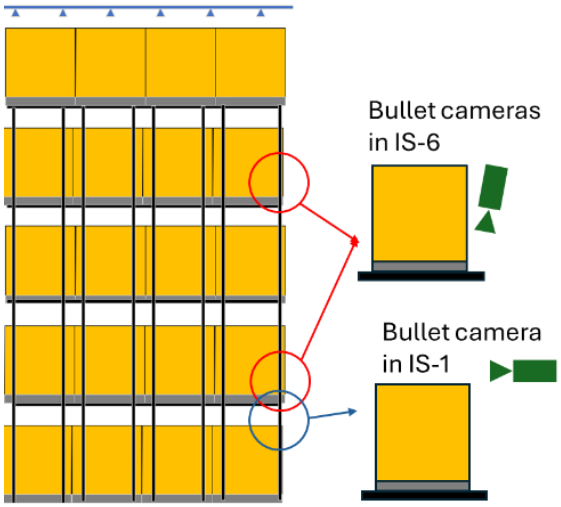

Figure 2-7: Illustration of bullet cameras positions

Table 2-1: Intermediate-scale test matrix of Phase 1

Test No.	Commodity	Water Density, mm/min (gpm/ft^2)	Nozzle Model	Special features
IS-1	Standard CUP	24 (0.6)	3/8HH20wsq	None
IS-2	Seamless CUP			
IS-3		33 (0.8)	1/2HH30wsq	
IS-4		52 (1.28)	1/2HH50wsq	
IS-5				Top ignition
IS-6				Angle iron
IS-7				Slope
IS-8		43 (1.05)	1/2HH30wsq	Top ignition

2.2 Numerical Methods

2.2.1 Model Development

The present work used FireFOAM, a computational fluid dynamics (CFD) solver, for numerical simulations. FireFOAM has been applied in numerous fire suppression modeling studies across various commodities [9, 10]. The framework for modeling water spray suppression of solid-fueled fires includes four major coupled components: 1) a gas-phase model [11, 12]; 2) a solid-phase pyrolysis model [13]; 3) a Lagrangian spray model; and 4) a water film model [14]. Model validations for separate physics have been performed in the corresponding referenced studies.

The pyrolysis model for CUP commodity is detailed in Ref. [15] and a brief explanation is provided here. Figure 2-8 (a) illustrates the interior of a pallet load of CUP commodity. Each box contains 125 plastic cups arranged in a 5×5×5 grid. The cups are separated by single-wall cardboard dividers. The pyrolysis model abstracts these inner structures using the "unit-cell" concept, which represents one plastic cup and half of the cardboard divider shared with its neighbors. This unit-cell has been studied in the Fire Propagation Apparatus (FPA) to determine its burning characteristics [15], which are embedded in the CUP pyrolysis model and coupled to separate model for the outer cardboard liner, characterized in Ref. [16]

In the model, the unit-cells are divided into two groups based on their location, as shown in Fig. 2-8 (b). Different modeling strategies are applied to different unit-cells and regions. For cardboard boxes and wood pallets, a 1-D pyrolysis model is used to simulate heat conduction and pyrolysis. When the cardboard burns through, the outer unit-cells are exposed to fire. For the inner unit-cells, the mass of all the cells is grouped into one unit as shown in Fig. 2-8 (c). After being heated to its ignition

temperature, all the unit-cells are modeled using a 0-D approach, with the fuel vapor mass generation rate per unit area, $\dot{\omega}_v''$ calculated as

$$\dot{\omega}_v'' = \frac{\dot{q}_{net}''}{\Delta H_{gas}}, \quad \text{2-1}$$

where $\dot{q}_{net}''$ is the net heat flux and ΔH_{gas} is the heat of gasification.

The heat fluxes vary in different regions and burning stages, as shown in Fig. 2-9. Initially, when the cardboard is intact, the convective heat flux, $\dot{q}_{conv.,cardboard}''$ is calculated based on the cardboard surface temperature, and the outer unit cells representing plastic cups are heated from the conduction of the cardboard. When the cardboard is consumed more than 50%, the convective heat flux to the unit cells is assigned a prescribed value of $\dot{q}_{conv.,unitCell}''$ = 15 kW/m^2. The radiation to the commodity, $\dot{q}_{rad.,in}''$ is calculated using a constant radiative fraction and the radiation emission, $\dot{q}_{rad.,em}''$ from the commodity is based on the unit cell bulk temperature. It is assumed that the outer unit cell ignites when its bulk temperature reaches a predefined threshold. Since flames inside the unit cells are not resolved, their contribution is effectively modeled by adding additional heat flux terms, $\dot{q}_{f,ouc}''$ and $\dot{q}_{f,iuc}''$, for outer and inner unit cells, respectively. These heat fluxes are determined from bench-scale FPA studies [15].

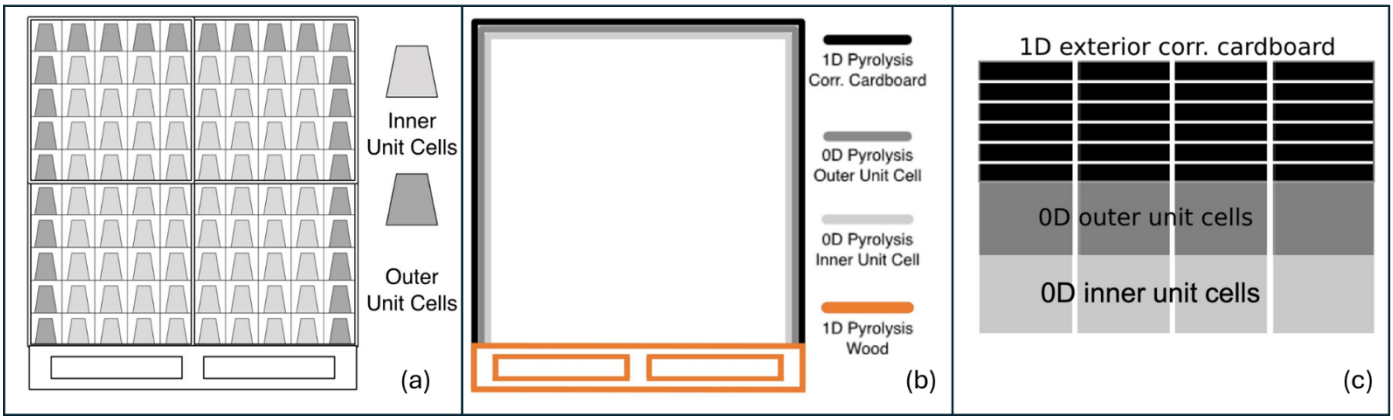

Figure 2-8: Framework of the simplified CUP pyrolysis model

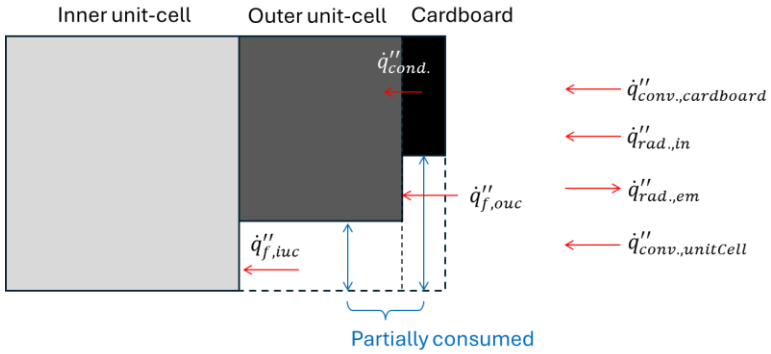

Figure 2-9: Illustration of heat fluxes to the cardboard and unit cells

The suppression model for CUP commodity generally follows the previous work for the Class-2 commodity [9, 10], where water films cool down the solid surface, block the heat fluxes and quench the pyrolysis of the solid fuels. A few changes were introduced to model the water transport between seams which was critical for MRR storage in a closed array. For standard CUP, water can flow through the seams between the boxes on each pallet load, as well as the seams between adjacent pallet loads, as illustrated in Fig. 2-10(a). The narrow seam permits water to pass through, thereby reducing the burning intensity under the wood pallets and on top of the boxes in the next tier down.

The width of the seam is on the millimeter scale, which is much smaller than the gas phase computational mesh size. Therefore, the seam cannot be directly modeled through the computational mesh, and a different modeling approach was taken, as shown in Fig. 2-10(b). First, a water mass sink is created in the water film region at the seam locations on top of the boxes. Next, droplets are injected at a location very close to the bottom surfaces with a small upward velocity, enabling them to wet the bottom surfaces. When enough water accumulates at the bottom surface, it will drip down to wet the lower tiers. The droplet injection location can be chosen within the pallet (in the small gaps between wood slabs) to achieve a similar wetting effect as observed in the test. The water transport time through the seam is modeled as

$$t_{seam} = H_{CUP}/U_{seam}\ , \qquad 2\text{-}2$$

where H_{CUP} is the height of the CUP commodity without the pallet, and U_{seam} is the seam water flow velocity. The value of U_{seam} is calibrated based on experimental observations of the water transport time from Test IS-1.

The water flow rate through a seam depends on both the amount of water available at the seam location and the width of the seam. When the seam width is sufficiently large (e.g., on the order of a few millimeters), the water flow rate near the top of the seam is usually insufficient to fully fill the gap. In this case, water flows along both vertical surfaces of the gap. The width of the seam is inherently random in realistic scenarios. To account of the coexistence of both very narrow seams (where boxes touch each other) and wider seams, an effective maximum seam flow rate (per unit length of the seam) is considered as

$$\dot{m}'_{seam,max} = 2\rho U_{seam} d_{film,max}\ , \qquad 2\text{-}3$$

where $d_{film,max}$ is the film thickness of free water flow on a vertical cardboard surface, and ρ is the water density. In this study, the thickness of a free surface flow on vertical cardboard surfaces uses 0.5 mm (0.02 in.), which is observed from the simulation of free surface water flows.

Gas phase combustion is modeled using an eddy dissipation concept model with ethylene as a surrogate fuel due to the unknown composition of the pyrolysis gases. To account for the substitution, the fuel mass flow rate is converted based on the heats of combustion of the fuels, given by $\dot{m}''_{C2H4} = \dot{m}''_{CUP}\Delta H_{c,CUP}/\Delta H_{c,C2H4}$, where $\Delta H_{c,CUP}$ and $\Delta H_{c,C2H4}$ are the heats of combustion of CUP pyrolysate and ethylene, respectively. The CUP pyrolysate includes cardboard and polystyrene cups, and its heat of combustion varies in different burning stages. When the cardboard is burning, $\Delta H_{c,CUP} = \Delta H_{c,cardboard}$. When the local cardboard is consumed, the heat of combustion at that location switches to the value of polystyrene cups, $\Delta H_{c,CUP} = \Delta H_{c,ps}$. The combustion process is modeled using a single-step reaction, with the consideration of flame extinction, given by

$$C_2H_4 + F_{RV}(3O_2 + 11.28N_2) \rightarrow F_{RV}(2CO_2 + 2H_2O + 11.28N_2) + (1 - F_{RV})C_2H_4^*\ , \qquad 2\text{-}4$$

where $C_2H_4^*$ is the quenched fuel and F_{RV} is the reactive volume fraction of the fuel, which is calculated using the flame extinction model described in Refs. [17, 18].

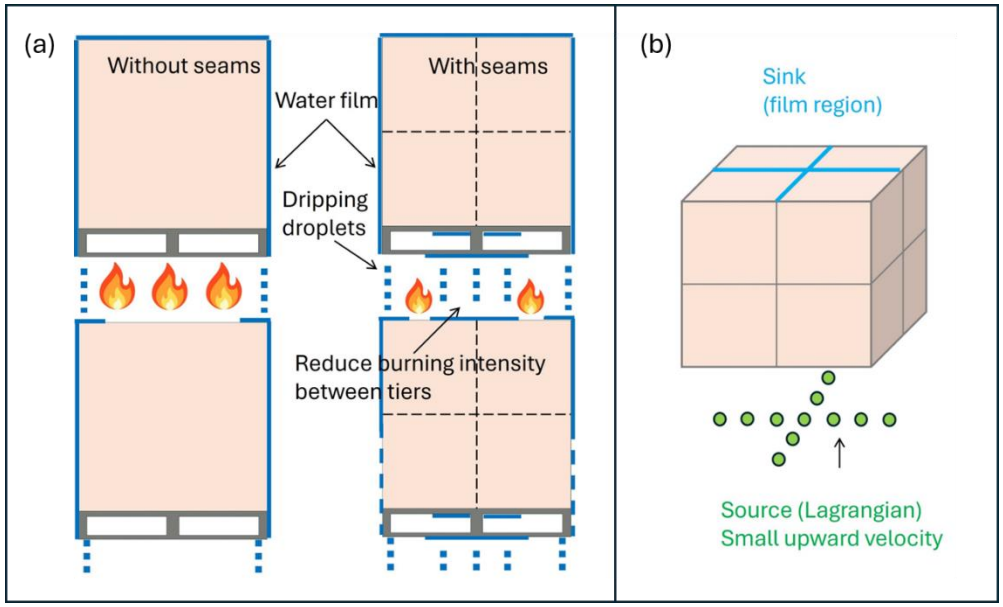

Figure 2-10: Illustration of seam water flow and its modeling approach

Radiation is calculated using a simple radiative fraction model. A global radiative fraction was assumed, which varies with time based on the gas phase fuel composition to avoid tracking and modeling multiple fuels at the same time. The global radiative fraction is blended with two fuels, given by

$$\chi_{r,global} = Y_{box,global}\,\chi_{r,box} + Y_{ps,global}\,\chi_{r,ps}\,, \qquad 2\text{-}5$$

where $\chi_{r,box}$ = 22% and $\chi_{r,ps}$ = 46% are the pyrolysate radiative fraction of the cardboard box and polystyrene cups, respectively, and $Y_{box,global}$ and $Y_{ps,global}$ are the area-integrated mass flow rate fraction of the two fuels.

2.2.2 Simulations of Intermediate-Scale Tests

Numerical simulations of the intermediate-scale tests were performed for IS-1 through IS-5. The simulation setup, including ignition conditions, duplicated those in the tests. The mesh setup for the MRR array used a 0.4 m (16-in.) background mesh with four levels of grid refinement, as shown in Fig. 2-11. At the center of the array, a 25-mm (1-in.) grid was used to model the fire growth and suppression. The mesh sizes used for different regions were (in million-cells) 4.5 for gas-phase, 7.5 for boxes of CUP, 6.9 for wood pallets, and 0.8 for water film. Simulations were conducted on an FM in-house cluster, with AMD EPYC-7452 (2.35 GHz) nodes. Each case used 64 processors. The simulation timespan per case was approximately 5,700 CPU hours to achieve 240 seconds of physical time.

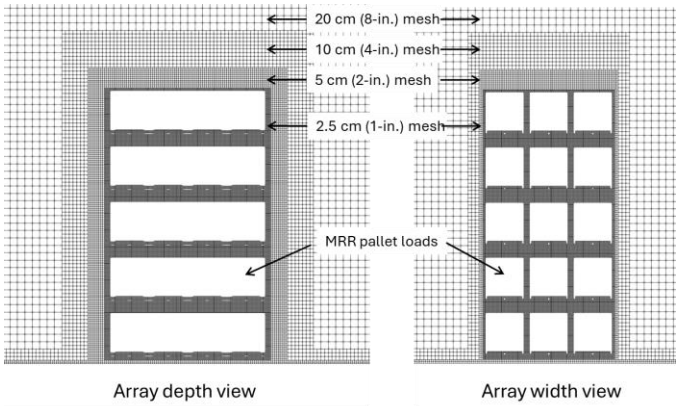

Figure 2-11: Mesh setup for simulations of the intermediate-scale MRR tests

Two additional simulations were performed on a 5-tier open DRR array to evaluate the influence of using seamless CUP commodity in a DRR array: one with standard CUP and another with seamless CUP. The mesh setup was the same as described above (see Fig. 2-12). Ignition was initiated at the center of the array near the ground level.

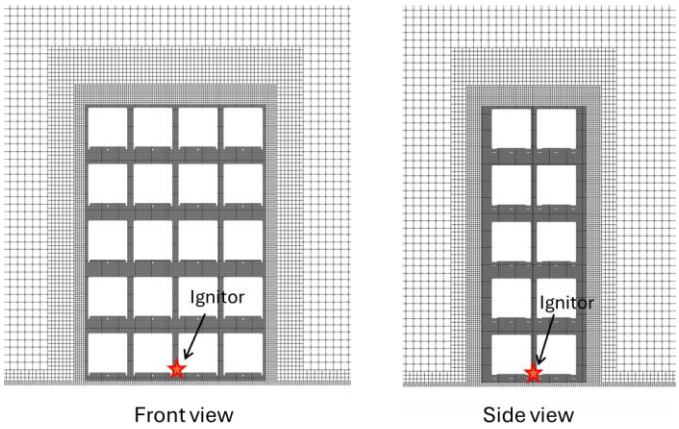

Figure 2-12: Mesh setup for simulations using a 5-tier DRR array

2.3 Results and Discussion

2.3.1 Influence of Seam Flow on Fire Suppression

Figure 2-13 shows a comparison of chemical HRR data from Tests IS-1 (standard CUP) and IS-2 (seamless CUP) used to evaluate the impact of seam flow in fire suppression of MRRs. The first peaks of HRR occur at similar times, indicating little impact on fire growth between the two CUP types. However, the HRR curves respond differently to the same water flux. The HRR for standard CUP drops after reaching a maximum of about 8 MW and remains under 2 MW after 05:00 (min:s). The HRR for seamless CUP also drops from a maximum of about 7 MW to 4 MW but increases thereafter, exceeding 12 MW at the time of test termination.

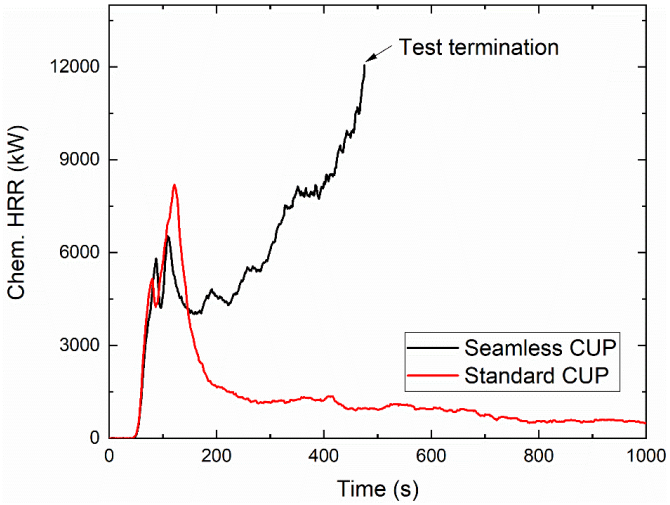

Figure 2-13: HRR comparison between Tests IS-1 and IS-2 using standard CUP and seamless CUP, respectively

Figure 2-14 shows images from Test IS-1 at various times. After ignition, the fire developed around the ignition location, vertically through the top of the array and laterally towards the left side of the array as well as two pallet-loads wide towards the right side. Water application was triggered around 00:53 and effectively suppressed fire growth to the bottom two tiers as shown by the image at 02:04. After 07:00, the flame spread into the third tier at the face of the array, which diminished

gradually over the next 20 minutes, under the continuous water application. This result suggests that the CDF of a 5-tier MRR storage is no greater than that of a DRR storage when using the standard CUP commodity, i.e. 23 mm/min (0.58gpm/ft^2).

However, the seamless CUP commodity appeared to have a higher CDF, as shown in Fig. 2-15. Similar initial fire growth was observed before water application started around 00:57 in Test IS-2. Unlike the effective suppression seen in Test IS-1, the fire size was still substantial around 02:17, burning commodities in the bottom three tiers. The fire also spread laterally over three pallet loads and reached the right side of the array. By 07:00, the fire was burning in all five tiers, resulting in a HRR of 12 MW. At that point, the test was terminated to avoid damage to the apparatus.

The comparison between Tests IS-1 and IS-2 suggests a greater challenge for MRR fire protection using seamless CUP commodity. One of the potential reasons could be the lack of water transport within the seams, leading to many dry spots in the clearance space between each tier, particularly at lower tiers in the array. The bullet camera installed between the first and second tiers captured the water flow through the seams in the standard CUP which, in addition to the flow over the vertical faces of the commodity, wets the top (horizontal) surface of the next lower tier, as shown in Fig. 2-16. This seam flow seemed to play a critical role in preventing the lateral spread that was observed when seamless CUP was used in Test IS-2. The bullet camera view also provided an approximate measurement on the seam flow velocity. After water application, it took about 20 seconds for water to flow through the seam to the bottom of the second tier. On average, it took about 5 seconds for water to pass through the seam of one tier. Therefore, the seam flow velocity U_{seam}, was set to 0.2 m/s (0.66 ft/s) in numerical simulations.

The impact of seam flow on the open DRR was investigated through modeling using a 5-tier array. The model-predicted HRR is shown in Fig. 2-17. Similar to the MRR, seam flow aids in suppression, but the difference is less pronounced compared to the closed MRR array. This can be attributed to the water film flow from the faces of the pallets wetting areas on the top of the lower tiers, as shown in Fig. 2-16 and illustrated in Fig. 2-18. In the open DRR array, the dry area on the lower tier, which cannot be directly wetted by the film water flow, is relatively small even without the seam flow. In contrast, the closed MRR array has a larger dry area, resulting in stronger burning between tiers. In addition, the open DRR array makes flame spread across the flue more difficult, even with a slightly higher HRR using the seamless CUP commodity. In the closed MRR array, the enhanced burning between tiers of the seamless CUP promotes lateral flame spread, making fire suppression more challenging. This explains why the closed MRR array is more sensitive to the seam water flow.

Figure 2-14: Images of various times during Test IS-1 using standard CUP commodity under water application rate of 24 mm/min (0.6 gpm/ft^2)

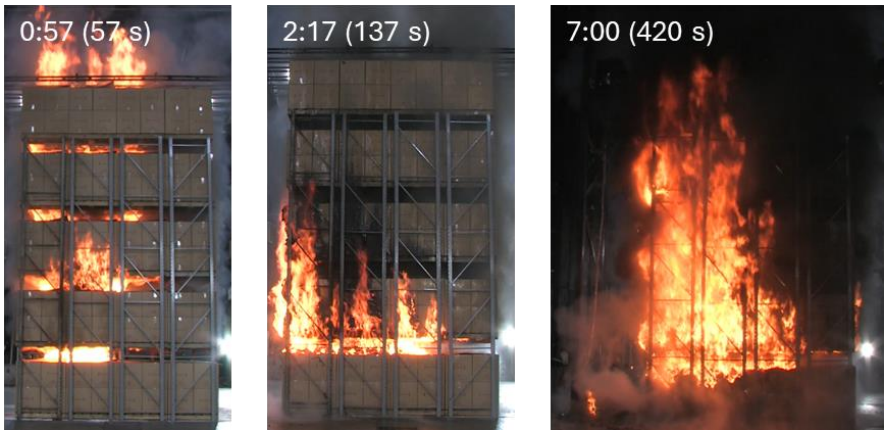

Figure 2-15: Images at various times during Test IS-2 using seamless CUP commodity under water application rate of 24 mm/min (0.6 gpm/ft^2)

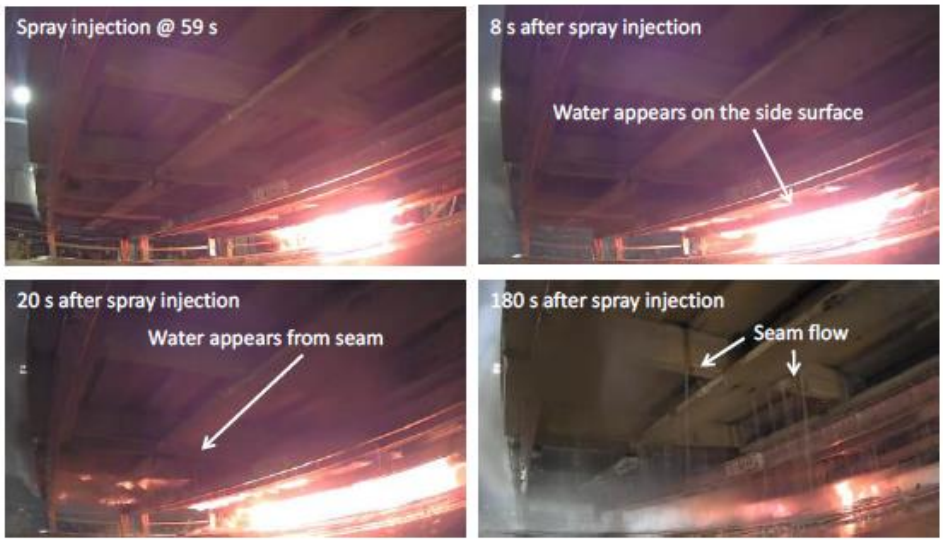

Figure 2-16: Bullet-camera view between first and second tiers in Test IS-1

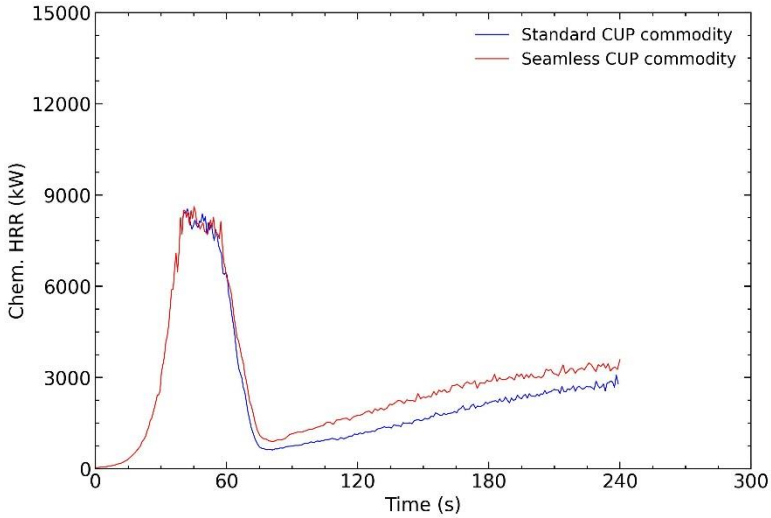

Figure 2-17: Comparison between standard and seamless CUP commodities in a DRR array using model predictions at 24 mm/min (0.6 gpm/ft^2) water density.

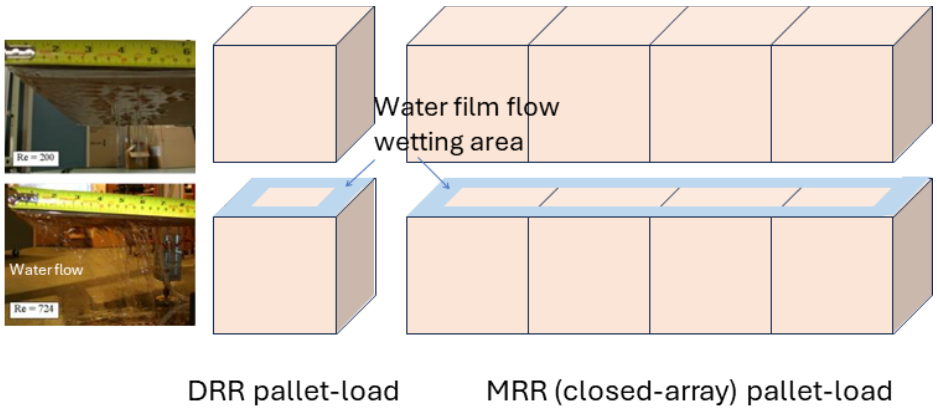

Figure 2-18: Illustration of water film wetting to lower tiers for DRR and MRR arrays (right) caused by the "curling" effect in the water transport (left photo shows water flow pattern along the bottom surface of the cardboard boxes with different flow Reynolds number defined as $Re = \dot{m}'/\mu_{water}$, where $\dot{m}'$ is the mass flow rate per unit length, μ_{water} is the water dynamic viscosity).

2.3.2 Fire Suppression Behavior under Varying Water Density

Figure 2-19 shows the HRRs of Tests IS-2, IS-3, and IS-4 using a water flux of 24 mm/min (0.6 gpm/ft^2), 33 mm/min (0.8 gpm/ft^2), and 52 mm/min (1.28 gpm/ft^2), respectively. With the increase of water application, Tests IS-3 and IS-4 were run for 30:00, with the HRR remaining below 10 MW throughout each test. However, like Test IS-2, the HRR increased after dropping upon the initial water application in both tests. After the second peak around 15:00 to 18:00, the HRR decreased again with the depletion of fuel.

Figure 2-20 shows the images from Test IS-3 at various times. The water application time and the corresponding fire size were similar to those of Tests IS-1 and IS-2. After water application, the fire was suppressed in the top tiers but persisted in the bottom two tiers. The amount of water delivered to the bottom tiers appeared insufficient to control the lateral flame spread, resulting in the flame spreading throughout those tiers over the next 10 minutes, shown by the images taken at 12:30 and 18:00.

Figure 2-21 shows the images from Test IS-4 at various times. The fire development and suppression processes within the first two minutes were again similar to those of Tests IS-2 and IS-3. However, the fire size at 04:00 was significantly reduced and the lateral flame spread was confined within the two pallet loads around ignition (left half of the array). While a surge in fire spread was observed around 16:00, the result suggests an effective fire suppression at this water flux shown by the image taken at 37:00. This is likely due to the strong shielding effect from the seamless CUP commodity.

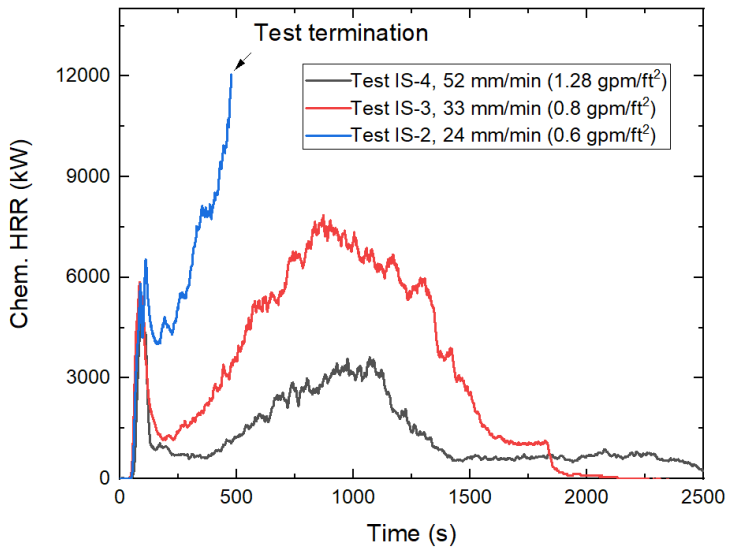

Figure 2-19: Heat release rate comparison between Tests IS-2, IS-3, and IS-4 comparing different water fluxes

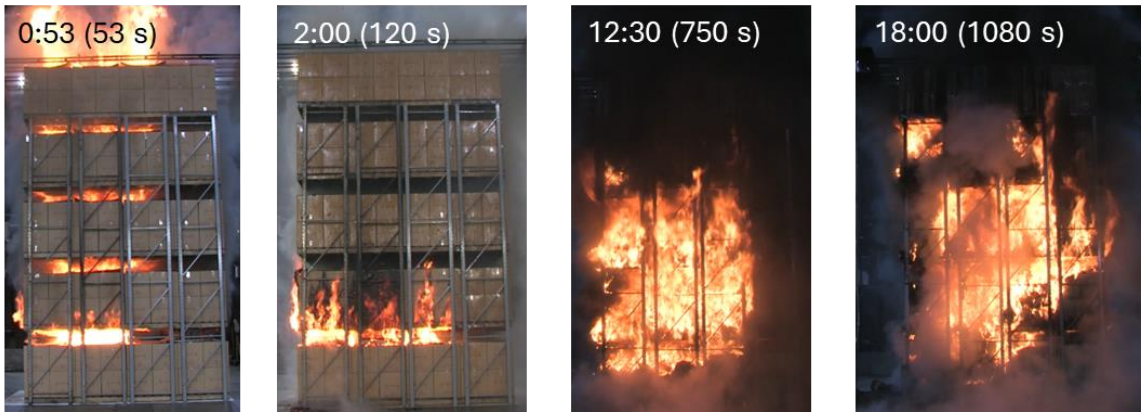

Figure 2-20: Images at various times during Test IS-3 using seamless CUP commodity under water application rate of 33 mm/min (0.8 gpm/ft^2)

Figure 2-21: Images at various times during Test IS-4 using seamless CUP commodity under water application rate of 52 mm/min (1.28 gpm/ft^2)

2.3.3 Influence of Angle Irons

Figure 2-22 shows the HRR data from Test IS-6 where angle irons were used, compared against those from Test IS-4 as the baseline test with the otherwise same configuration and same water flux. The peak HRR before water application at 01:18 was about 7 MW, slightly larger than that in the baseline test. The HRR decreased rapidly after the water application, but the rate of decrease slowed after 02:00 at around 2 MW. The HRR reached the same level as that in Test IS-4 by around 30:00, but unlike IS-4 there was no clear second peak in fire size at intervening times.

Figure 2-23 shows images from Test IS-6 at various times. The flame spread before water application is similar to the baseline test, but the subsequent fire suppression was less effective at the bottom three tiers. Notably, the fire was more persistent within the second and third tiers. However, such difference did not influence the result around 10:00 where flame spread was confined around the ignition location under the top tier.

Figure 2-24 shows images from the IR camera, the bullet camera installed on top of the angle iron at the fourth tier, and the bullet camera installed on top of the second tier. The IR camera captured a small water stream coming out of the angle iron at the top tier, but nothing from the lower tiers. The bullet cameras confirmed this finding, with a few droplets from the fourth tier and nothing from the second tier. The overall results suggest that the angle iron may direct some water at the top tier to the aisle, but such impact does not substantially increase the CDF. The increased fire size could be due to typical stochastic variation in large-scale testing.

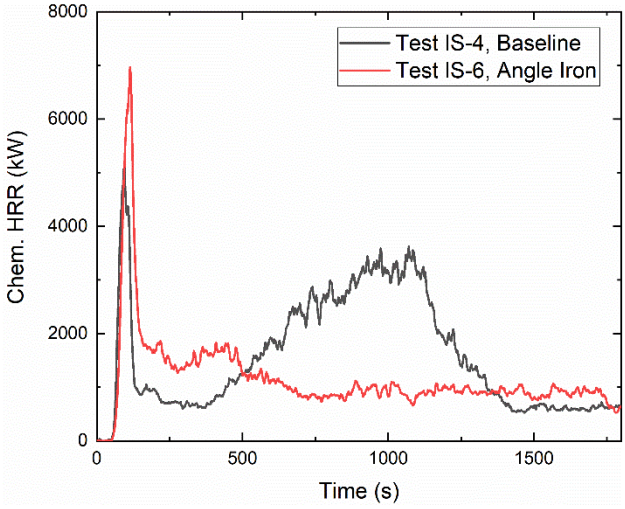

Figure 2-22: Heat release rate comparison between Tests IS-4 and IS-6 comparing presence of angle irons

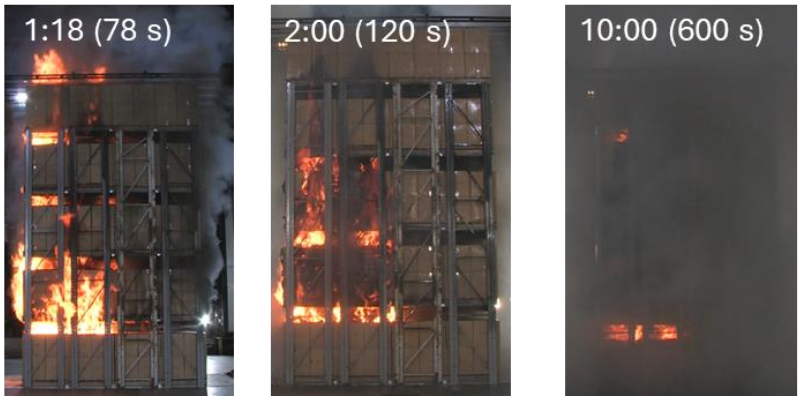

Figure 2-23: Images at various times during Test IS-6 in presence of angle irons

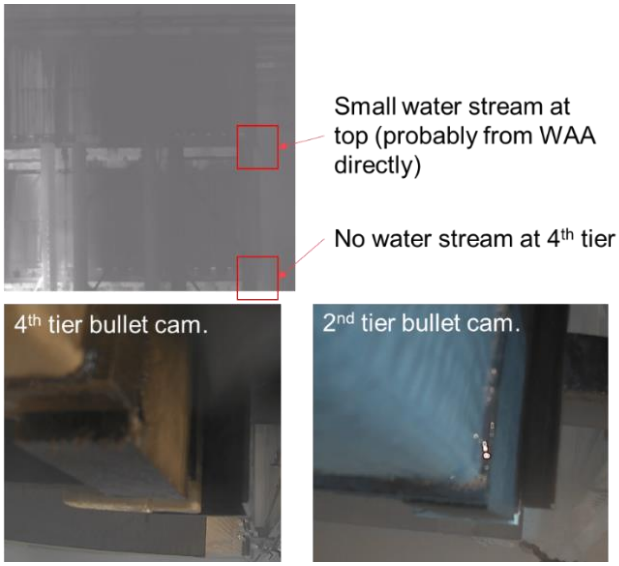

Figure 2-24: Images from the IR camera and bullet cameras of Test IS-6 in presence of angle irons

2.3.4 Influence of Rack Slope

Figure 2-25 shows the HRR from Test IS-7 where a sloped rack was used. The HRR trend is almost identical to the baseline test for the first 25:00 after ignition. After that, Test IS-7 shows a third peak in the HRR data around 30:00, which is due to re-establishment of the fire at the array face. Figure 2-26 shows a series of images taken during Test IS-7, with flame spread behavior exhibiting little difference in the presence of a slope. The only notable difference was due to the breakout of fire at the third tier around 25:00, which diminished shortly after the two pallet loads of commodities were consumed, as shown by the image taken at 34:00. Figure 2-27 shows the images from the IR camera and the remote camera, capturing a water stream coming out of the top tier. No water stream was found in lower tiers. This is probably the result of a large amount of water impinging on the top surface of the array from the nozzles and forming a water film flowing towards the lower end. Similar behavior did not happen in lower tiers because the water was more distributed over vertical surfaces from tier to tier.

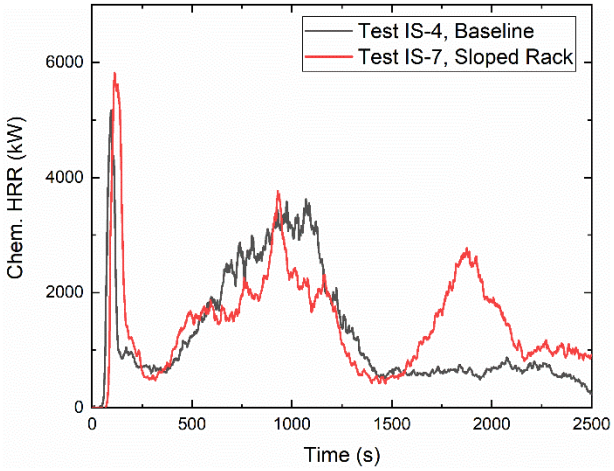

Figure 2-25: Heat release rate comparison between Tests IS-4 and IS-7 comparing presence of rack slope

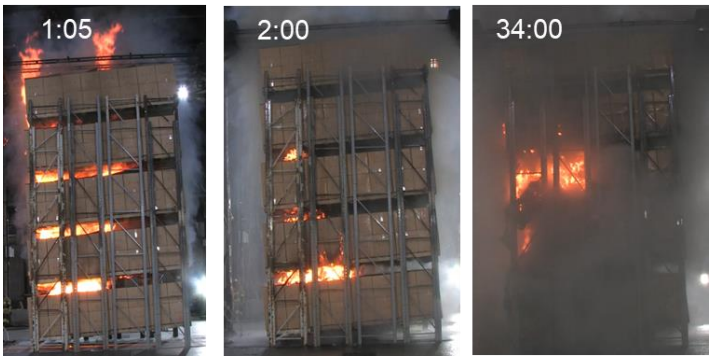

Figure 2-26: Images at various times during Test IS-7 in presence of sloped rack

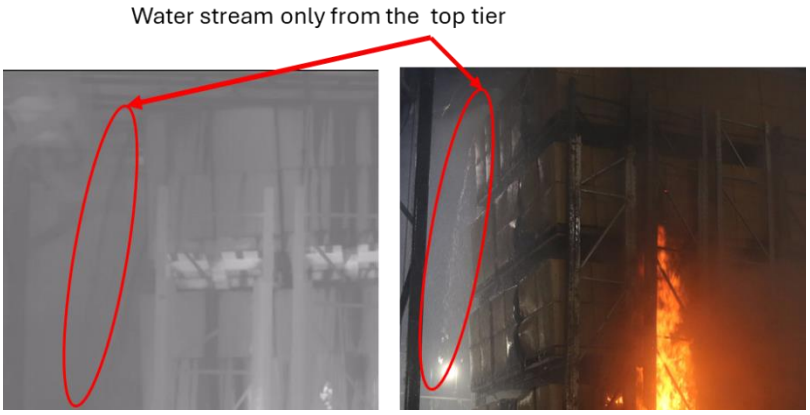

Figure 2-27: Images from the IR camera and the remote camera of Test IS-7 in presence of sloped rack

2.3.5 Influence of Ignition Location

Figure 2-28 shows a comparison of HRR data between Tests IS-4 and IS-5 using different ignition locations (flue vs. top). While some quantitative differences are noticed such as the peak HRR, there is no conclusive evidence to suggest one is more challenging than the other. This is possibly due to the small array used in the intermediate-scale tests or the large water application rate that diminishes the impact of ignition location. Additional numerical simulations were conducted to compare the flue and top ignition cases in a larger-scale configuration to verify the worst-case scenario for testing. The simulations showed that top ignition delays the sprinkler activation, resulting in a larger HRR before sprinkler activation, and requiring more activations to control the fire. A detailed discussion is provided in Section 2.3.7, together with other large-scale simulations for conciseness.

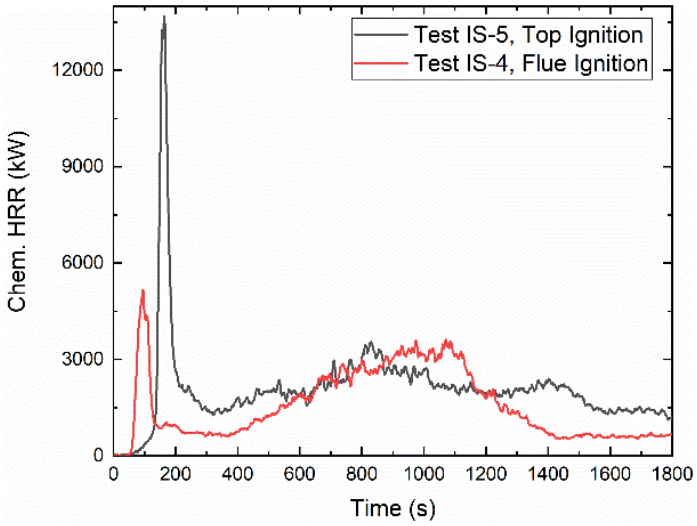

Figure 2-28: Heat release rate comparison between Tests IS-4 and IS-5 comparing different ignition locations

2.3.6 Required Delivered Density

Figure 2-29 shows the HRR from Tests IS-5 and IS-8 with water application rate of 52 mm/min (1.28 gpm/ft^2) and 43 mm/min (1.05 gpm/ft^2) respectively. Based on the initial test series (IS-3 through IS-5), the required delivered density (RDD) for 5-tier MRR storage could only be bounded loosely: Test IS-3 indicated that the RDD must be greater than 33 mm/min (0.8 gpm/ft^2), while Tests IS-4 and IS-5 suggested that it should be less than or equal to 52 mm/min (1.28 gpm/ft^2). This range was too broad to support confident engineering judgment. The inclusion of the successful fire-controlled result from Test IS-8 significantly narrowed the RDD range, reducing it to between 33 mm/min (0.8 gpm/ft^2) and 43 mm/min (1.05 gpm/ft^2) for 5-tier MRR storage. The corresponding RDD for 7-tier MRR storage was then estimated to lie between 46 mm/min (1.12 gpm/ft^2) and 60 mm/min (1.47 gpm/ft^2) using a linear extrapolation of the 5-tier results. It should be noted that a more realistic extrapolation would likely exhibit a more gradual slope than a simple origin-based linear trend, consistent with critical delivered flux correlations for standard CUP commodities in DRR storage [8]. As such, the projected RDD range for 7-tier MRR storage should be interpreted as a conservative estimate.

The estimation of RDD can be of great help in the design of large-scale tests, in conjunction with actual delivered density (ADD) calculations. The ADD describes the amount of sprinkler discharged water reaching the top of the storage after penetrating a fire plume of given size, represented by its convective HRR. A typical adequate sprinkler protection will require the ADD in under-1 sprinkler configuration to be larger than the RDD of a specified storage height. Figure 2-30 shows comparisons of ADD values for different sprinkler designs against the estimated RDD for 7-tier MRR storage. Two representative sprinklers were selected for K240 lpm/bar$^{1/2}$ (K16.8 gpm/psi$^{1/2}$) and K360 lpm/bar$^{1/2}$ (K25.2 gpm/psi$^{1/2}$) sprinklers, respectively. Four-sprinkler designs were used, including two protection recommendations for CUP commodity and one for uncartoned expanded plastic (UEP) commodity listed in FM Data Sheet 8-9 [1]. The remaining condition is an equivalent-flow design of K360 lpm/bar$^{1/2}$ (K25.2 gpm/psi$^{1/2}$) at 2.8 bar (40psi) using K240 lpm/bar$^{1/2}$ (K16.8 gpm/psi$^{1/2}$) sprinklers. The upper and lower bounds of the horizontal bars are calculated using convective HRRs of 500 kW and 1000 kW respectively, which represent a reasonable fire size at the first sprinkler activation based on large-scale tests of CUP commodity stored in a 7-tier DDR storage under a 12.2-m (40-ft) ceiling. The ADD values were calculated using a machine-learning based model [19, 20]. Note that the convective HRRs (fire size) was used to account for the penetration loss in large-scale tests with a given ceiling clearance. This is different from the fire size used in intermediate-scale tests to account for the enhanced suppression effectiveness with all nozzles open at the same time compared with a sequential sprinkler activation.

The comparisons suggest that protection using K240 lpm/bar$^{1/2}$ (K16.8 gpm/psi$^{1/2}$) at 3.6 bar (52 psi) will likely be inadequate, while protection using K360 lpm/bar$^{1/2}$ (K25.2 gpm/psi$^{1/2}$) at 5.2 bar (75 psi) will have a better chance to control the fire. The two other protection designs may have a marginal chance to achieve adequate protection depending on the actual value of RDD.

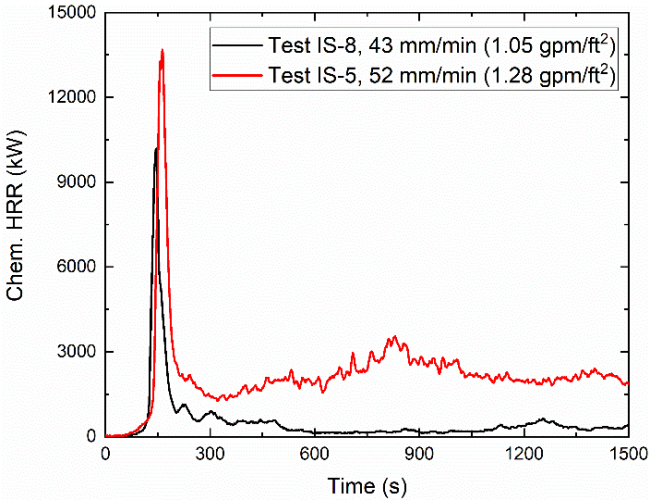

Figure 2-29: Heat release rates from Tests IS-5 and IS-8

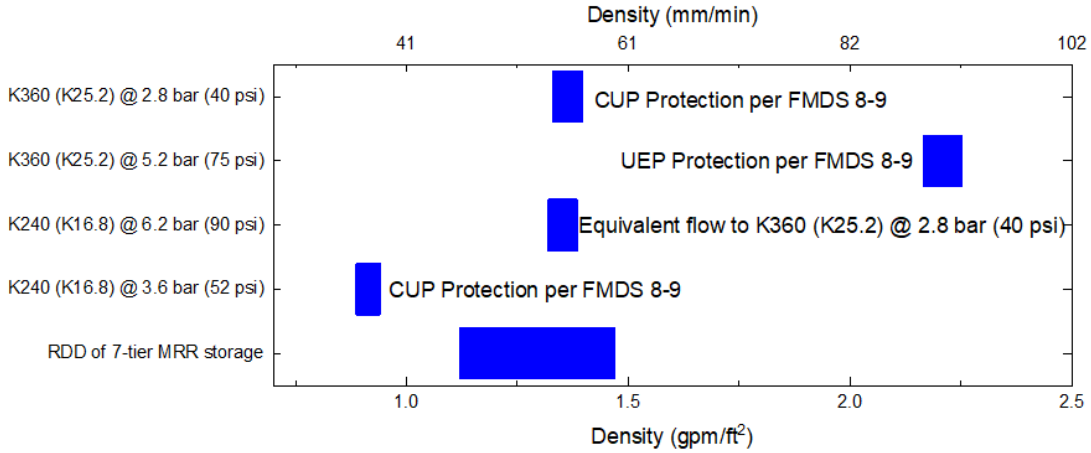

Figure 2-30: Comparison of ADD for different sprinkler designs for CUP commodity against RDD of 7-tier MRR storage (Note that the 7 tier RDD is estimated by extrapolation)

2.3.7 Numerical Model Validation

Figure 2-31 shows a comparison of HRR data from Tests IS-1 and IS-2 and their corresponding simulations ISS-1 and ISS-2 using standard CUP and seamless CUP with the flue ignition scenario. The simulated HRR trends are time-shifted to align with the measured data at the time of reaching a HRR value of 1,000 kW to minimize the influence of variations in time delay for incipient fire development. A modeled free-burn HRR curve is also included to illustrate that, without water suppression, the fire would escalate rapidly, exceeding 20 MW in less than two minutes.

In the tests, water application was triggered manually based on pre-defined criteria (see description in Section 2.1), with the fire size at activation roughly 5 MW (for the flue ignition case). The activation criteria used in the tests were not modeled in the simulation; instead, the water application time was approximated by averaging the maximum HRRs of Tests IS-1 and IS-2 among both first and second peaks, which was about 7 MW for the flue-ignition case. For other flue ignition cases, the same activation time was used for consistency. For the top ignition case, the water application began when the modeled fire size reached the peak HRR of Test IS-5, approximately 14 MW. Prior to water application, the modeled HRR closely matched the measured values, demonstrating strong model performance in predicting the fire growth rate for the CUP commodity.

The simulation for Tests IS-1 and IS-2 show similar trends compared with the tests, though with a faster decay of HRR after water application. The qualitative agreement indicates that the model successfully captures the key physics of both standard CUP and seamless CUP commodities.

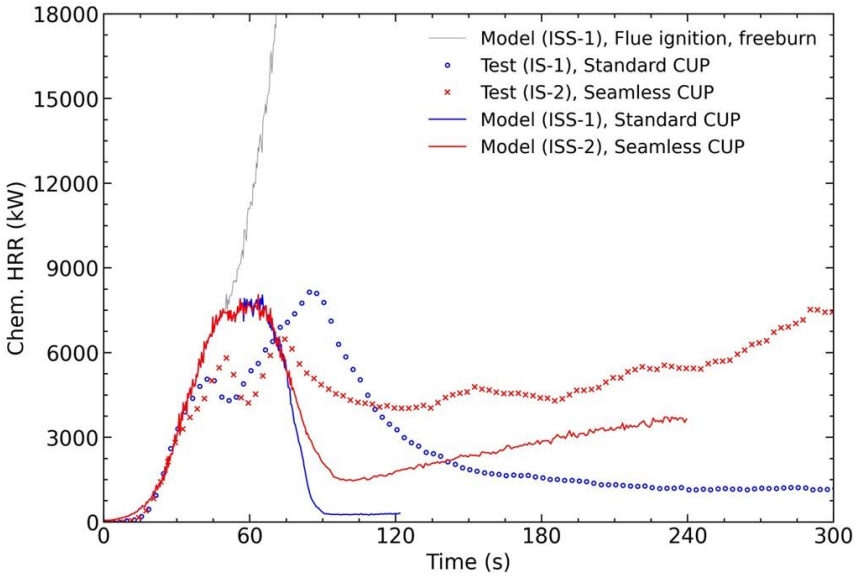

Figure 2-31: Comparison of chemical HRRs between simulations and tests using standard and seamless CUP

Fig. 2-32 shows a visual comparison of Test IS-2 and the corresponding simulation just before water application from (a) the front view and (b) the side view, as well as (c) after water application. The simulation is in good agreement with the test in term of the vertical and horizontal extent of the fire during both the free-burn and suppression stages. Similar agreement was observed for Test IS-1.

Figure 2-33 compares chemical HRR from simulations and tests of seamless CUP commodity in MRR storage under varying water application fluxes. The simulations capture the general trends well, where a rapid drop in HRR after water application is followed by an increase or plateau region depending on water density. The fact that the simulations captured the transition from controlled (Test IS-4) to uncontrolled (Tests IS-2 and IS-3) outcomes provides a high degree of confidence in the validity of the model.

Figure 2-34 compares chemical HRR data from simulations against their corresponding tests when (IS-4 and IS-5) using different ignition locations under a water density of 52 mm/min (1.28 gpm/ft^2). The different fire growth patterns observed in the tests are again well captured by the simulations. The simulations show that in the top ignition case, the fire initially spreads laterally under the wood pallets, which take longer to ignite than the cardboard boxes, and hence the fire growth is slower compared with the flue ignition case. After about one minute, the fire begins to grow vertically in two transverse flues, leading to a rapid increase in the HRR.

Figure 2-35 shows a comparison of fire images before water application from (a) the front view and (b) the side view, as well as (c) after water application, between Test IS-5 and its corresponding simulation. The vertical and lateral flame spread before water application is again well captured by the simulation. In addition, the confinement of the fire within the center row on the second tier after 8 minutes is also well captured in the simulation.

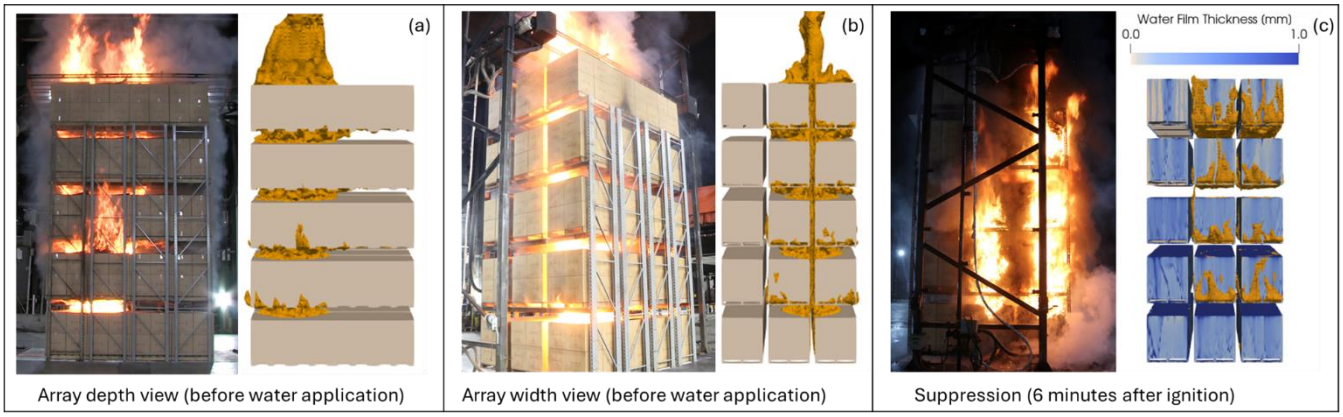

Figure 2-32: Comparison of fire sizes before water application from (a) the front view and (b) the side view, as well as (c) after water application, between Test IS-2 and its corresponding simulation ISS-2

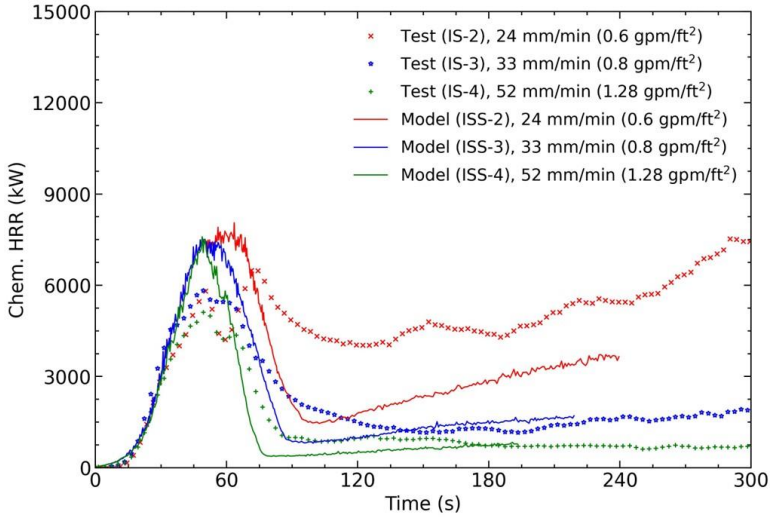

Figure 2-33: Comparison of HRR data between simulations and tests using seamless CUP under different water densities

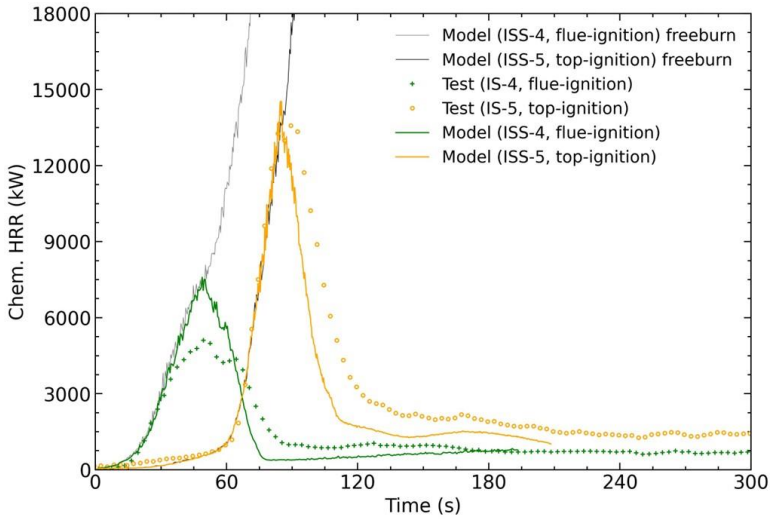

Figure 2-34: Comparison of chemical HRR data between simulations and tests using different ignition locations

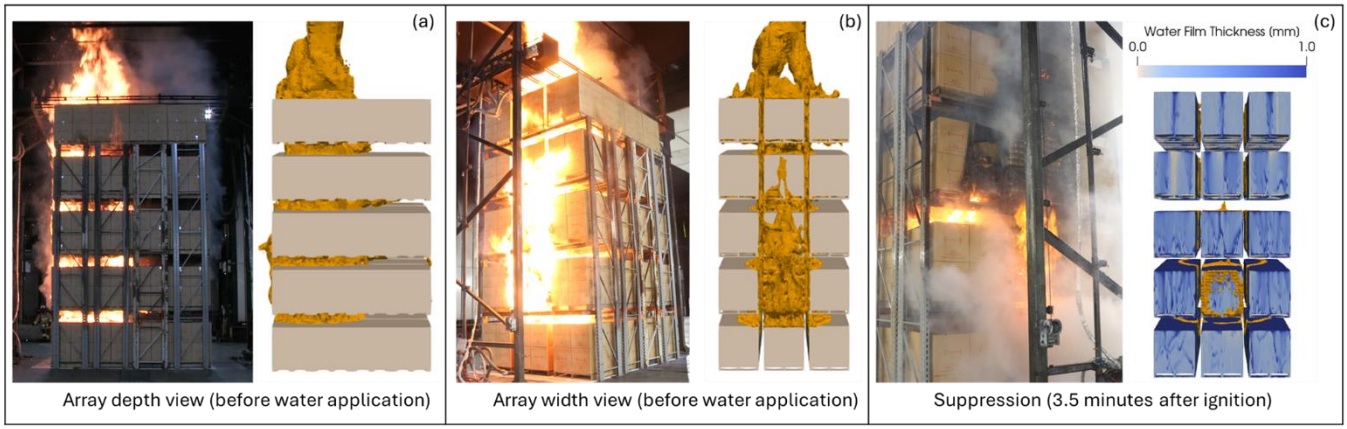

Figure 2-35: Comparison of fire sizes before water application from (a) the front view and (b) the side view, as well as (c) after water application, between Test IS-5 and its corresponding simulation ISS-5

2.3.8 Recommendations for Phase 2

Phase 1 achieved several key results, which were used to develop plans for Phase 2. First, numerical models were developed and validated for MRR storage using intermediate-scale fire suppression tests. These models provided a tool to support large-scale fire test designs in Phase 2. Second, parametric studies were conducted using the intermediate-scale tests and numerical models to determine appropriate representative configurations for use in the large-scale tests. The studies showed that 1) seamless CUP should be used as a conservative option for protection evaluation of MRR in closed array storage; 2) special features like angle iron and sloped rack have minimal impact on fire suppression and do not need to be included in the large-scale tests; and 3) ignition on top of the first tier generates a more challenging fire scenario compared to ignition in a flue space. Finally, the RDD analysis showed that the existing protection guidance using K240 lpm/bar$^{1/2}$ (K16.8 gpm/psi$^{1/2}$) at 3.6 bar (52 psi) would likely yield inadequate protection. Using K360 lpm/bar$^{1/2}$ (K25.2 gpm/psi$^{1/2}$) sprinklers at 5.2 bar (75 psi) was identified as a potential starting point to design adequate protection for 7-tier MRR storage.

3. Phase 2: Evaluating Protection

3.1 Numerical Configuration

Numerical simulations were carried out prior to testing to support the protection design. These simulations examined various configurations, including ignition location, sprinkler layout, sprinkler pressure, seam flow rate, and other relevant parameters. The simulated results were used to identify the worst-case scenarios for testing and to evaluate the suppression performance of different design options. Insights gained from the modeling effort helped reduce the number of large-scale tests required without compromising the effectiveness of the evaluation.

To accelerate the simulation, the model set up a narrower array of six rows and excluded the target arrays. To assess the influence of ignition location on sprinkler performance, both top and flue ignition scenarios were considered. These arrangements, with array dimensions, are illustrated in Fig. 3-1(a), along with representative computer-rendered views of the simulated storage array during the early suppression stage [see Fig. 3-1(b) and (c)]. Note that in the simulations, only the central array was modeled, while surrounding arrays were artificially generated for visualization purposes. Table 3-1 summarizes the 7-tier array simulations performed in this study.

The relative position of the sprinklers to the ignition location can influence the initial activation pattern. Subsequent activation timing may be affected by spray cooling, which can lead to sprinkler skipping and impact overall suppression performance. Based on past testing experience, ignition occurring between two sprinklers with a 2-ft offset is usually the most challenging case. For this scenario, two configurations were examined: ignition between sprinklers aligned in the east-west (E-W) (LSS-2 and LSS-4) direction and ignition between sprinklers aligned in the north-south (N-S) (LSS-1 and LSS-3) direction, as illustrated in Fig. 3-2.

After identifying the most challenging ignition scenario—top ignition between two sprinklers along the E-W direction (LSS-4)—the modeling explored the effects of sprinkler K-factor and discharge pressure. Simulation LSS-5 evaluated the feasibility of ceiling-only sprinkler protection by using the maximum design available for DRR protection. Simulations LSS-6 and LSS-7 explored alternative protection designs for existing facilities using K240 lpm/bar$^{1/2}$ (16.8 gpm/psi$^{1/2}$) sprinklers. More specifically, simulation LSS-6 evaluated the possibility of utilizing the elevated pressure delivered to the first one or two sprinklers in practical scenarios to achieve suppression. Note that the pressure was set to a fixed value during the simulation and the pressure decay (that would occur in reality) was not modelled. Simulation LSS-7 then altered the closed array to a semi-open array by introducing a 2.5-cm (1-in.) gap between pallets in an attempt to reduce the hazard. The sprinkler suppression modeling cases are summarized in Table 3-1, where the underlined cases indicate the recommendations for large-scale testing.

The mesh configuration for the large-scale test simulations followed the same strategy used in the intermediate-scale test simulations in Phase 1, as shown in Fig. 3-3. A fine 2.5-cm (1-in.) grid was used within the fuel array region, while the resolution was coarsened to 5 cm (2 in.) in the ceiling plume region. Farther away from the array, the grid resolution was progressively reduced to manage computational resources. The mesh consists of approximately 20.2 million cells in the gas-phase region, 2.86 million cells in the water-film region, and 60.7 million cells in the solid-phase region. Simulations were run on FM's research high-performance computing cluster (AMD EPYC 9654, 2.4 GHz) utilizing 384 cores. A single simulation case required 30 to 40 days of runtime to produce nine minutes of physical time.

Figure 3-1: (a) Schematic of a plan view of the simulation setup, (b) front and (c) side elevation views showing computer-rendered MRR array, flame, and water flow (only center array is modeled, surrounding arrays were artificially generated and are included for illustration purpose)

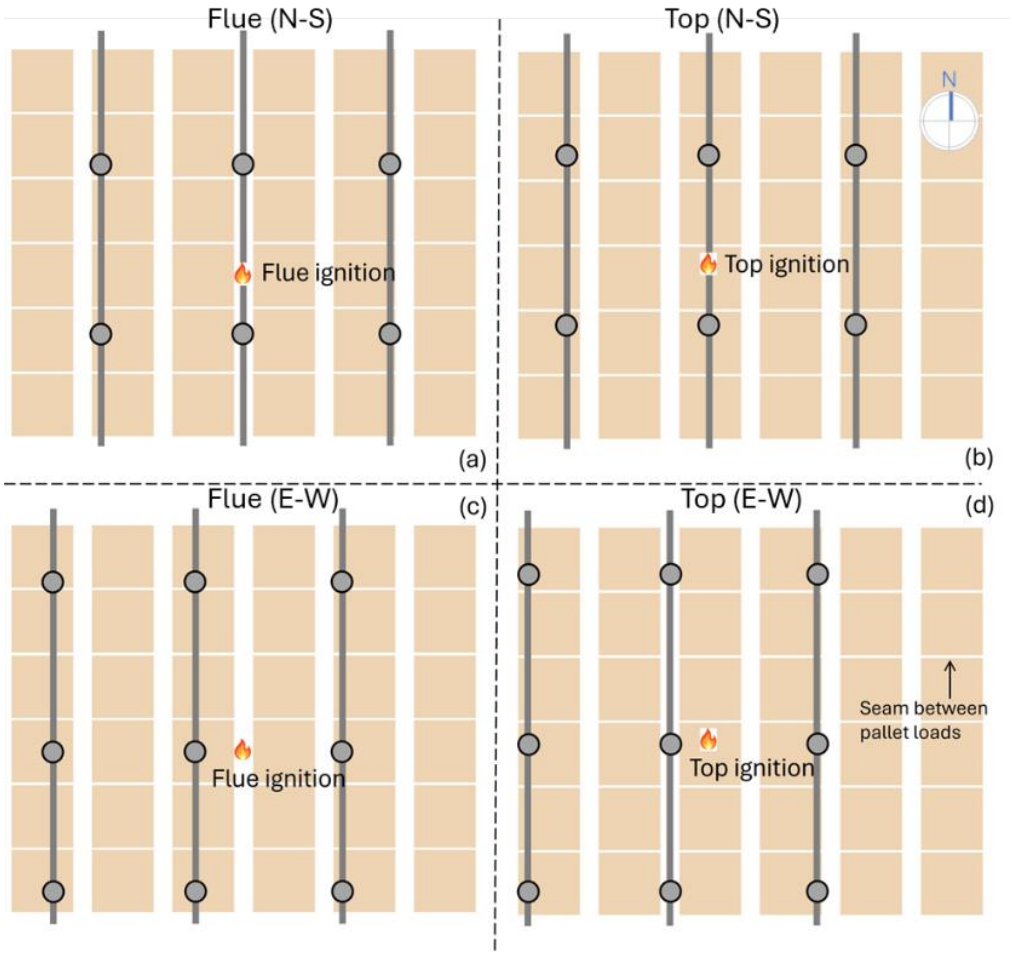

Figure 3-2: Plan-view schematic of the simulation setup for ignition locations and sprinkler array layouts relative to the ignition location: (a) flue ignition between two sprinklers along the flue, (b) top ignition between two sprinklers along the flue, (c) flue ignition between two sprinklers across the flue, and (d) top ignition between two sprinklers across the flue.

Table 3-1: Large-scale simulation matrix of Phase 2 (underlined cases recommended for large-scale testing)

Simulation No.	LSS-1	LSS-2	LSS-3	LSS-4	LSS-5	LSS-6	LSS-7
Ignition location	Flue (N-S)	Flue (E-W)	Top (N-S)	Top (E-W)			
Sprinkler K-factor, lpm/bar$^{1/2}$ (gpm/psi$^{1/2}$)	240 (16.8)				360 (25.2)	240 (16.8)	240 (16.8)
Pressure, bar (psi)	3.6 (52)				5.2 (75)	6.2 (90)	3.6 (52)
Gap between pallet loads, cm (in)	No						2.5 (1)
Predicted sprinkler activation	3	6	4	9	2	3	9
Test sprinkler activation	NA	NA	NA	19	1	2	NA

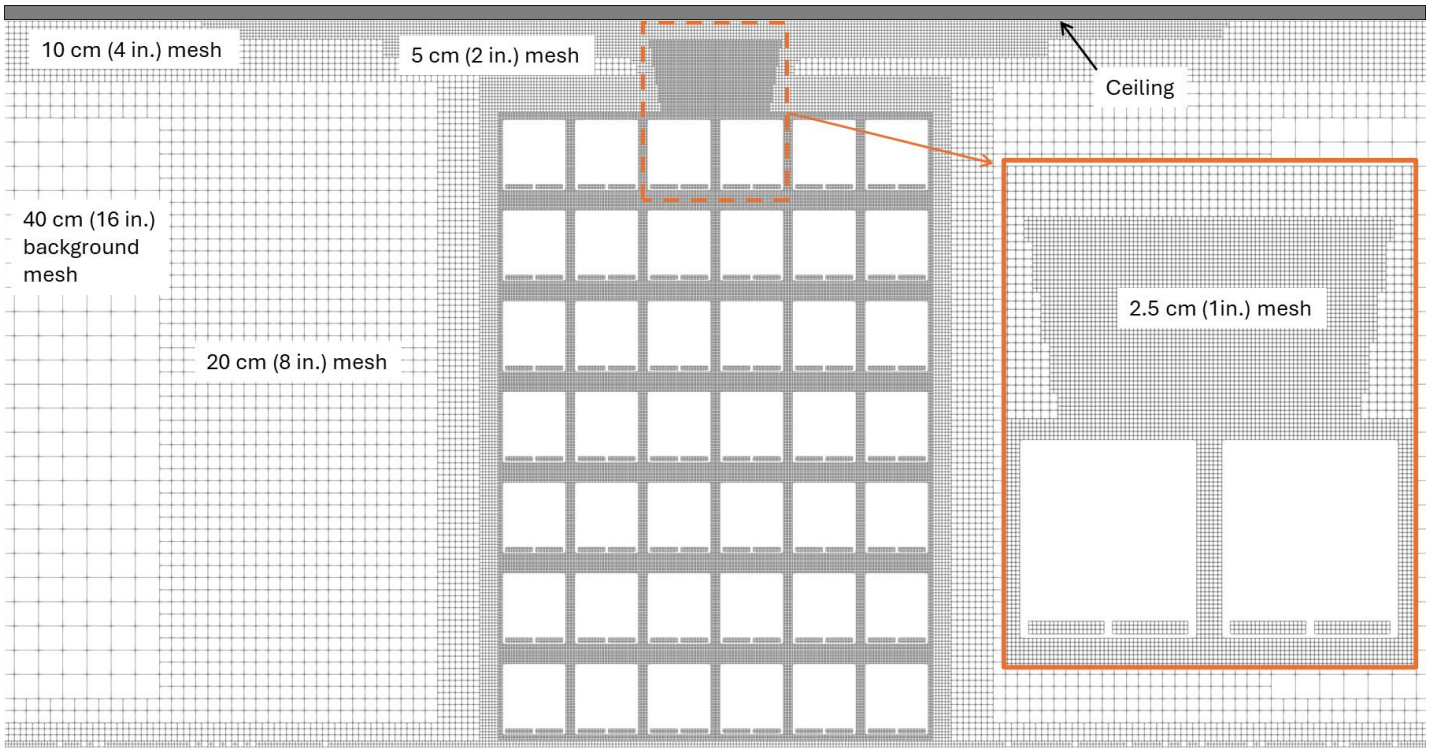

Figure 3-3: Mesh configuration for large-scale simulations, shown on a vertical cross-sectional plane through the center of the storage array.

3.2 Experimental Methods

Five large-scale fire tests involving seamless CUP commodity in a 7-tier MRR array were conducted under the north movable ceiling in the large burn laboratory at the FM Research Campus. The movable ceiling is 24.4 m (80 ft.) by 24.4 m (80 ft.) and was positioned at a height of 12.2 m (40 ft) above the floor in this work. The tests were conducted with an exhaust rate of 5,700 m^3/min (200,000 ft^3/min).

Figures 3-4 and 3-5 show plan and elevation views of the test array and corresponding sprinkler layout used in the first large-scale test (Test LS-1, see Table 3-2). Fifty-six sprinklers were installed on the ceiling with 3 m (10 ft) by 3 m (10 ft) spacing (shown as the blue dots in each figure), with a link-to-ceiling distance of 33 cm (13 in.). The protection design used K240 lpm/bar$^{1/2}$ (K16.8 gpm/psi$^{1/2}$) pendent, quick response sprinklers operating at 3.6 bar (52 psi), and providing an average density of 49 mm/min (1.2 gpm/ft^2).

The main array measured 11.1 m (36.5 ft) wide, 6.4 m (21 ft) deep, and 10.4 m (34 ft) tall, centered under the movable ceiling with 0.6 m (2 ft) offset to the east. The array consisted of seven tiers of storage on nine rows, separated by a net 15-cm (6-in.) flue where an absolute 23-cm (9-in.) flue was used across each 7.6-cm (3 in.) rack upright. Each tier was 1.5 m (5 ft) tall. Within each row, six pallet loads of commodities were butted against each other. Two target arrays were positioned on the north and south side of the main array, each separated by a 1.2-m (4 ft) aisle. Each target array was a single row rack of the same width and height as the main array with 15-cm (6-in.) flues. Seamless CUP commodity was used, represented by yellow boxes in both figures.

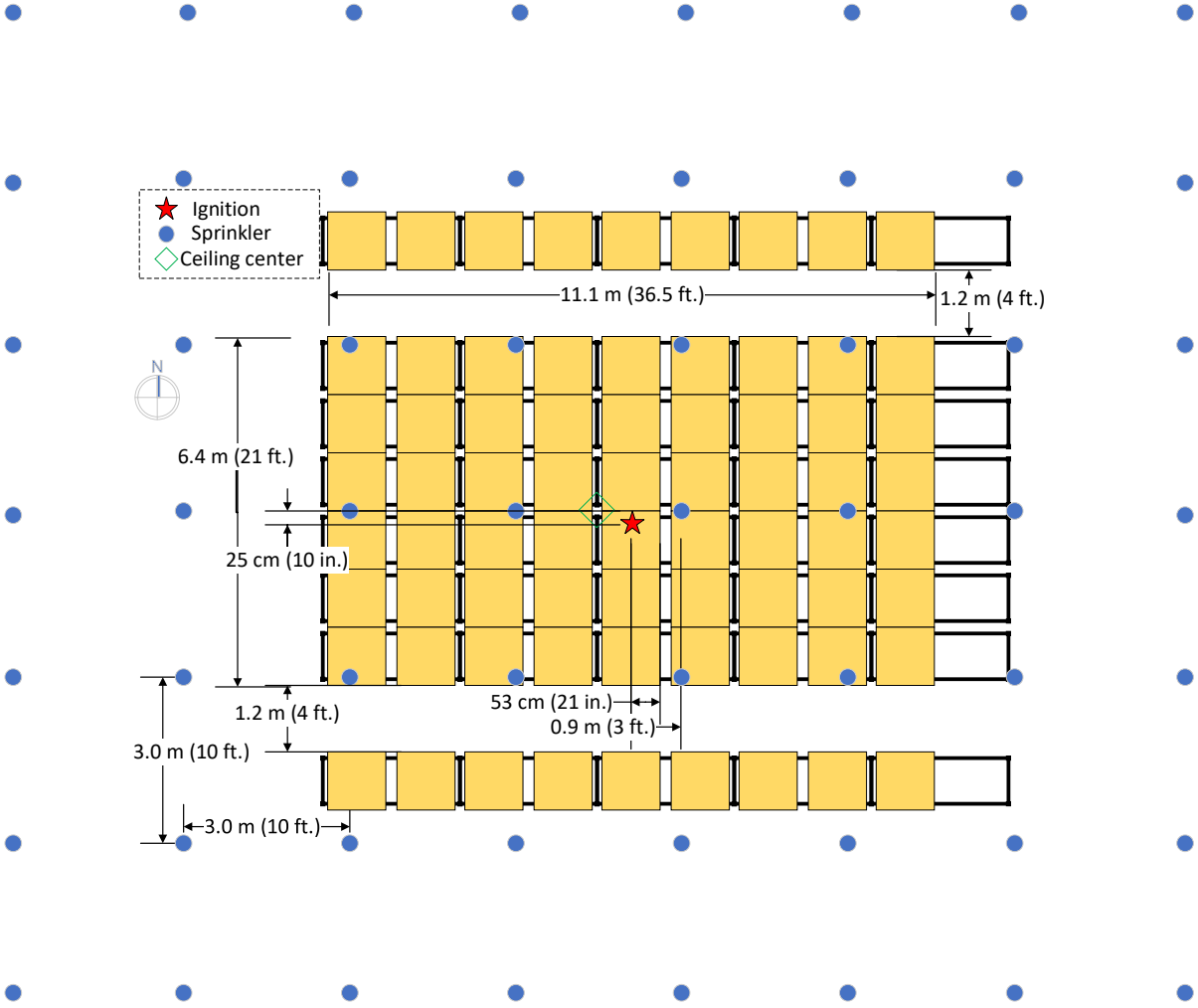

Figure 3-4: Schematic of a plan view of Test LS-1 setup

The top ignition configuration was used based on the results from Phase 1. One full ignitor was placed on top of the first tier along the center row, with a 25-cm (10-in.) offset toward the south. The offset minimized the influence of the rack beams which could slow down the lateral spread underneath the pallets. The ignitor was made of cotton cellulose material wrapped in cheesecloth, measuring 7.6 cm (3 in.) in diameter and 15 cm (6 in.) long. The ignitor was soaked with 240 mL (8 oz.) of gasoline and sealed in a clear plastic bag. A propane torch was used to light the ignitor, signaling the onset of the test.

Tests LS-2 to LS-5 used almost the same configuration, including the same commodity, ignition, and array arrangements. The differences are listed in Table 3-2. Tests LS-1 and LS-4 used K240 lpm/bar$^{1/2}$ (K16.8 gpm/psi$^{1/2}$) sprinklers operating at 3.6 bar (52 psi), with respective aisle widths of 1.2 m (4 ft) and 2.4 m (8 ft), both representing scenarios in existing facilities following the guidance of NFPA 13 and FM Data Sheet 8-9 [1, 2]. Test LS-5 was identical to Test LS-1 but with an elevated sprinkler discharge pressure of 6.2 bar (90 psi). Tests LS-2 and LS-3 used K360 lpm/bar$^{1/2}$ (K25.2 gpm/psi$^{1/2}$) sprinklers operating at 5.2 bar (75 psi) and 2.5 bar (40 psi), respectively. The corresponding sprinkler link-to-ceiling distances were adjusted in those

two tests from 33 cm (13 in.) to 42 cm (17 in.). The link-to-ceiling distance for each type of sprinkler was determined based on the maximum allowable distance specified in FM Data Sheet 2-0, *Installation Guidelines for Automatic Sprinklers* [21].

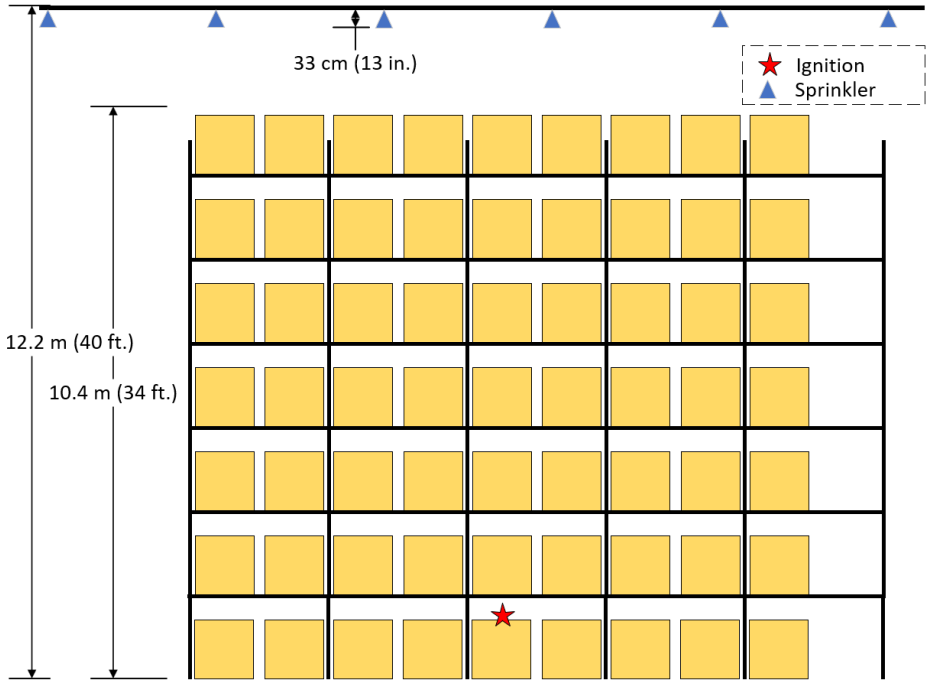

Figure 3-5: Schematic of an elevation view of Test LS-1 setup

Table 3-2: Large-scale test matrix of Phase 2

Test No.	LS-1	LS-2	LS-3	LS-4	LS-5
Sprinkler K-Factor, lpm/bar$^{1/2}$ (gpm/psi$^{1/2}$)	240 (16.8)	360 (25.2)	360 (25.2)	240 (16.8)	240 (16.8)
Link-to-ceiling distance, cm (in.)	33 (13)	43 (17)	43 (17)	33 (13)	33 (13)
Pressure, bar (psi)	3.6 (52)	5.2 (75)	2.8 (40)	3.6 (52)	6.2 (90)
Aisle space, m (ft)	1.2 (4)	2.4 (8)	2.4 (8)	2.4 (8)	1.2 (4)

All large-scale tests were recorded using both visible and IR video cameras and still photographs. The ceiling was instrumented with 125 exposed-junction, 0.8-mm (20-AWG), Chromel-Alumel (K-type) thermocouples, with a bead-to-ceiling distance of 15 cm (6 in.). The thermocouples had a response time index of 8.0 (m-s)$^{0.5}$ [14.5 (ft-s)$^{0.5}$]. At the ceiling center, nine additional thermocouples were embedded in a cross-shaped steel angle to measure temperatures representing the thermal response of ceiling structural elements. Ceiling sprinklers were equipped with electrical circuits based on a trip wire mechanism to determine individual sprinkler activation times. Water flow meters and pressure transducers were monitored during each test to ensure the sprinkler system was operated within the design range.

The results of each test were evaluated using ceiling steel temperature, extent of flame spread, and number of sprinkler activations as the primary criteria to determine the adequacy of the tested protection design. For adequate protection, the one-minute average ceiling steel temperature should not exceed 538°C (1,000°F). Beyond this threshold, steel loses roughly 50% of its load-bearing capacity, which could result in unacceptable damage to the building structure. No more than eight sprinklers should operate during each test, based on a 12-sprinkler design with a 50% safety factor. The sprinklers along the perimeter of the ceiling should not be operated, which would indicate potential for further activation if the test ceiling was larger and additional sprinklers were present. Finally, the extent of flame spread should be confined by the aisles without jumping to the target arrays, which would indicate the potential of further flame spread and additional sprinkler activations if the test array were larger. With all other criteria satisfied, if flame spread was well confined within the main array, the protection would be considered adequate and could be applied to storage arrays larger than that used in the test. However, if

the flame spread to the ends of the main array, the protection would still be considered adequate but with additional restriction that continuous storage areas would need to be limited to no greater than the length of the test array.

3.3 Results and Discussion

3.3.1 Model Predictions

Figure 3-6 shows the chemical HRR data from simulations LSS-1 to LSS-4, which investigated the worst-case scenario for ignition location. Predicted sprinkler activation times are indicated on the curves using circles. The top-ignition cases (LSS-3 and LSS-4) exhibited delayed initial fire growth and higher peak HRRs compared to the flue ignition cases (LSS-1 and LSS-2), consistent with the intermediate-scale results. Higher HRRs in the top ignition scenarios resulted in more sprinkler activations. Among these, the top ignition between two sprinklers along the east-west direction posed the greatest challenge with nine sprinkler activations and the largest fire. Note that these simulations did not include target arrays; if present, target ignition could have occurred in these scenarios, likely triggering additional sprinklers.

Figure 3-7 shows the modeled gas temperature in two vertical planes: (a) cutting through the array depth direction, and (b) cutting through the width direction, both in the top ignition case along the east-west direction (LSS-4). The array-depth contour reveals extensive lateral flame spread across multiple tiers, primarily due to the absence of longitudinal flues. Upon the first sprinkler activation, hot gases flowed to the front and back side of the array, preheating the vertical surfaces at the face of the array. If water density is inadequate, this preheating can quickly lead to face ignition. The array-width contour shows the simultaneous fire growth along two adjacent transverse flues, resulting in a larger burning area and a faster fire growth rate compared to the flue ignition case.

Figure 3-8 shows simulation results using the maximum ceiling-only protection design, i.e. K360 lpm/bar$^{1/2}$ (K25.2 gpm/psi$^{1/2}$) sprinklers operating at 5.2 bar (75 psi) (LSS-5), and a benchmark case using the existing recommendation of K240 lpm/bar$^{1/2}$ (K16.8 gpm/psi$^{1/2}$) sprinklers (LSS-4). Two sprinklers were activated and successfully controlled the fire when using the maximum design compared to nine and potentially more sprinklers in the benchmark case. Figure 3-9 shows simulation results with alternative options using K240 lpm/bar$^{1/2}$ (16.8 gpm/psi$^{1/2}$) sprinklers (LSS-6 and LSS-7). Increasing the pressure to 6.2 bar (90 psi) in LSS-6 improved suppression effectiveness, reducing the fire HRR and the number of sprinkler activations. Extended simulations showed HRR decay after 12 minutes without further activations. Introducing a small gap between pallet loads in LSS-7 also reduced HRR, but the number of sprinkler activations remained high. Considering the operational difficulty of enforcing a 1-inch gap and its limited benefit, using an elevated pressure was deemed a better option, to be validated with large-scale testing.

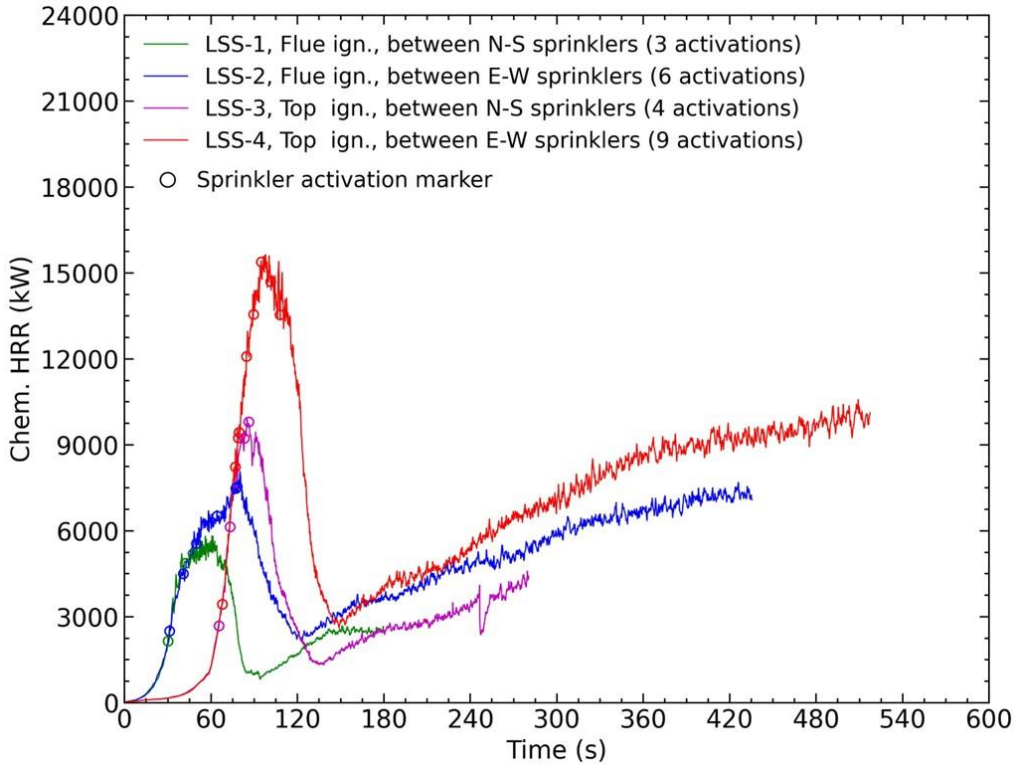

Figure 3-6: Model predicted HRRs comparing ignition and sprinkler locations (LSS-1 to LSS-4)

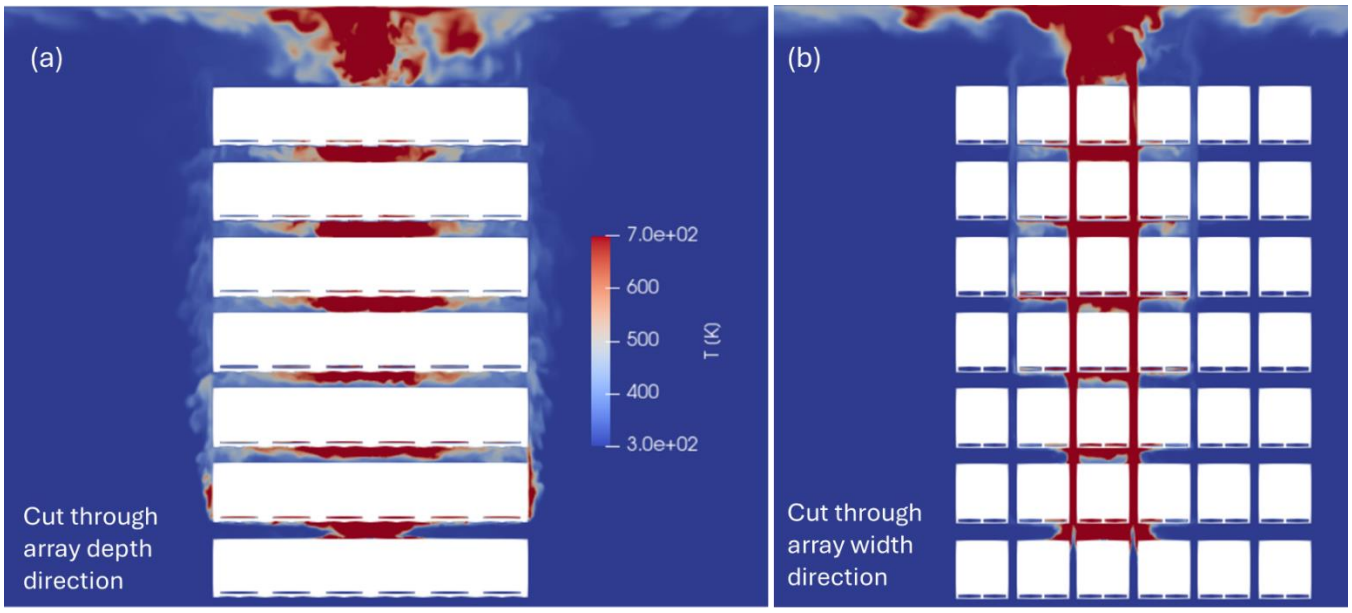

Figure 3-7: Model predicted gas phase temperature before the first sprinkler activation (LSS-4, the worst-case ignition scenario)

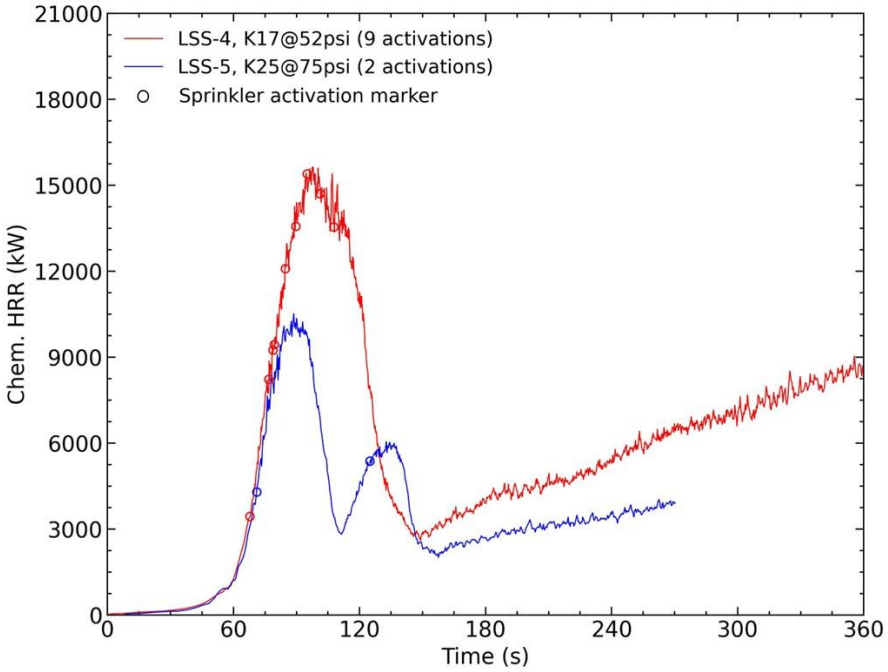

Figure 3-8: Model predicted HRRs comparing K240 lpm/bar$^{1/2}$ @ 3.6 bar (K16.8 gpm/psi$^{1/2}$ @ 52psi, LSS-4) and K360 lpm/bar$^{1/2}$ @ 5.2 bar (K25.2 gpm/psi$^{1/2}$ @ 75psi, LSS-5)

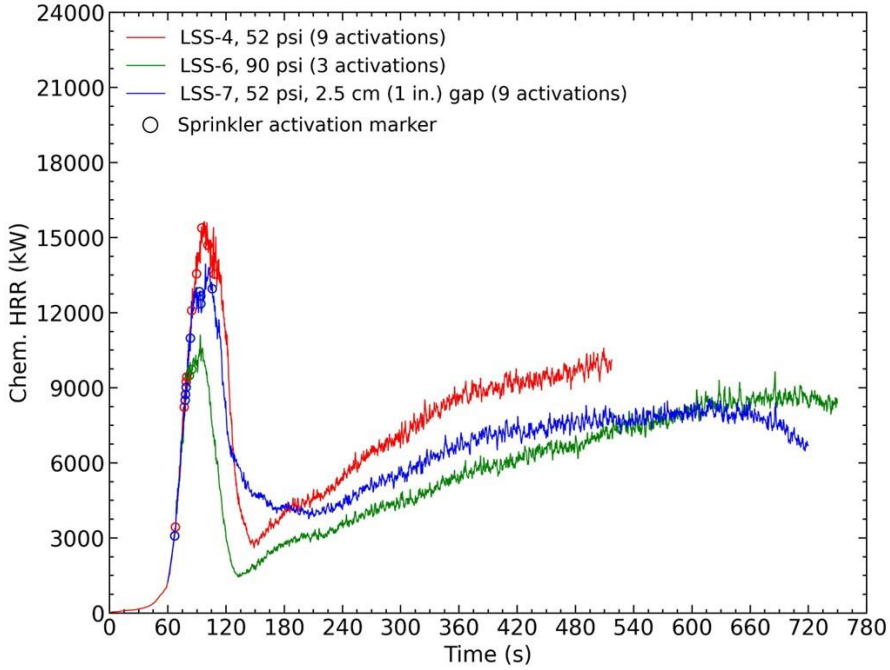

Figure 3-9: Model predicted HRRs comparing injection pressures (3.6/5.2 bar or 52/90 psi) and the gap between pallet-loads, K240 lpm/bar$^{1/2}$ (K16.8 gpm/psi$^{1/2}$) (LSS-5, LSS-6, and LSS-7)

3.3.2 Evaluating Current Protection Guidance for Existing Facilities (Large-Scale Tests 1, 4, and 5)

Figure 3-10 shows the sprinkler operation times and pattern of Test LS-1. The first sprinkler activated around 01:41, close to the ignition location. After activation, the vertical flame spread was temporally reduced in the east flue adjacent to the ignition location. However, the sprinkler water delivered to the west flue across the ignition location was insufficient to achieve the same effectiveness, resulting in the activation of the second sprinkler at 03:12. With the two sprinkler activations, flame

spread along the east-west direction seemed to be controlled, while flame spread underneath the pallets along the north-south direction continued. With the development of fire on the south face and subsequent ignition of the south target array, three more sprinklers above the south aisle activated around 06:05, and additional four sprinklers activated in the next four minutes. A similar process occurred on the north side of the array. The fire at the north face and target activated nine more sprinklers in less than two minutes. No further sprinkler activations were observed during the rest of the test, which was terminated at 30:00. During the test, sprinkler skipping patterns were found on both the south and north sides of the array. In addition, among the 19 sprinkler activations, five were at the perimeter of the ceiling, indicating a potential of further activations should the ceiling be larger than that used in the test.

Figure 3-11 shows images from Test LS-1 at times corresponding to the flame spread reaching the ends of the main array and jumping to the targets. Each image is stitched together at the orange line from photos taken by multiple cameras viewing the south and north aisles. The flame spread to the south end of the main array at 02:47, ignited the south target array at 06:02, and jumped to the north target array around 15:00 as shown by the IR images. This suggests that fire could spread further should there be more fuel across the south aisle. Similar processes were also found on the north side of the array, with flame spread to the north end of the main array at 05:42 and north target ignition at 10:43.

Figure 3-12 shows images taken after the test, including the manual firefighting at the north and south faces of the main array. The fire damage was limited along the east-west direction where commodities were separated by flues, but excessive along the north-south direction. In addition, fire damage in the upper tiers was limited to areas near the face of the array, especially for the top tier.

Figure 3-13 shows a schematic of estimated fire damage in each tier. The damaged area was estimated by viewing around the main array using a mobile lift platform. Note that the damage assessment was based on visual estimation without disassembling the array. The fire damage from lateral spread increased with the tier height and reached a maximum at the third tier. The damage in the upper tiers was limited, especially for the top tier. This observation agrees with the intermediate-scale test results, where the top tier was also well protected by direct water application. The overall extent of flame spread and corresponding damage were well controlled within the main array in the direction where commodities were separated by flues but reached both ends of the main array and extended to the target arrays along the other direction. This suggests a potential for uncontrolled flame spread should the storage array be larger than that used in the test.

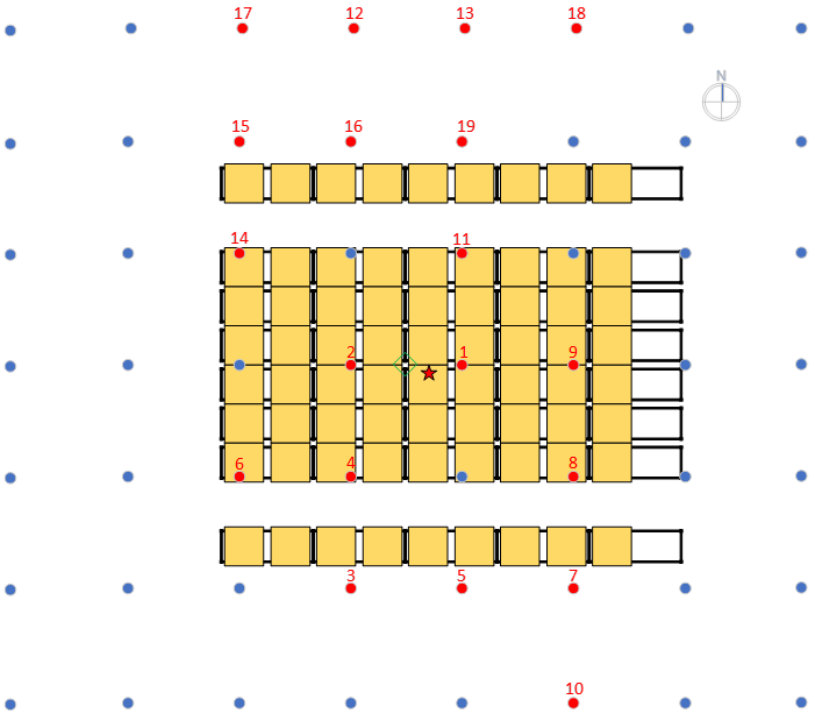

No.	Time (mm:ss)
1	1:41
2	3:12
3	6:05
4	6:05
5	6:09
6	6:18
7	7:57
8	8:47
9	9:58
10	10:00
11	10:37
12	11:00
13	11:01
14	11:04
15	11:12
16	11:23
17	11:56
18	12:11
19	12:12

Figure 3-10: Sprinkler operation times and pattern of Test LS-1

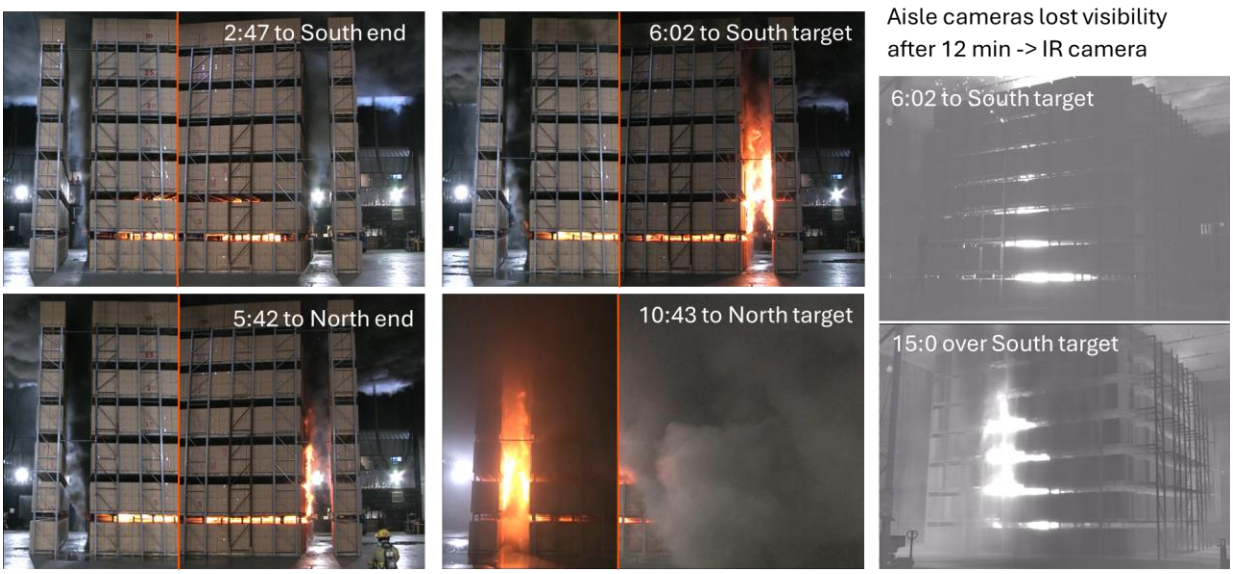

Figure 3-11: Images at various times during Test LS-1

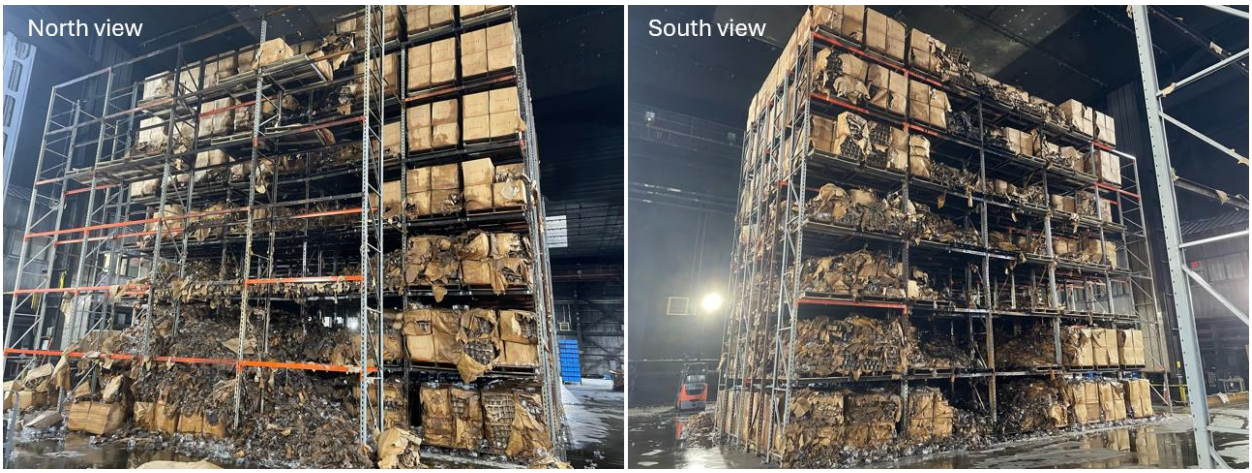

Figure 3-12: Images taken after test for damage assessment of Test LS-1

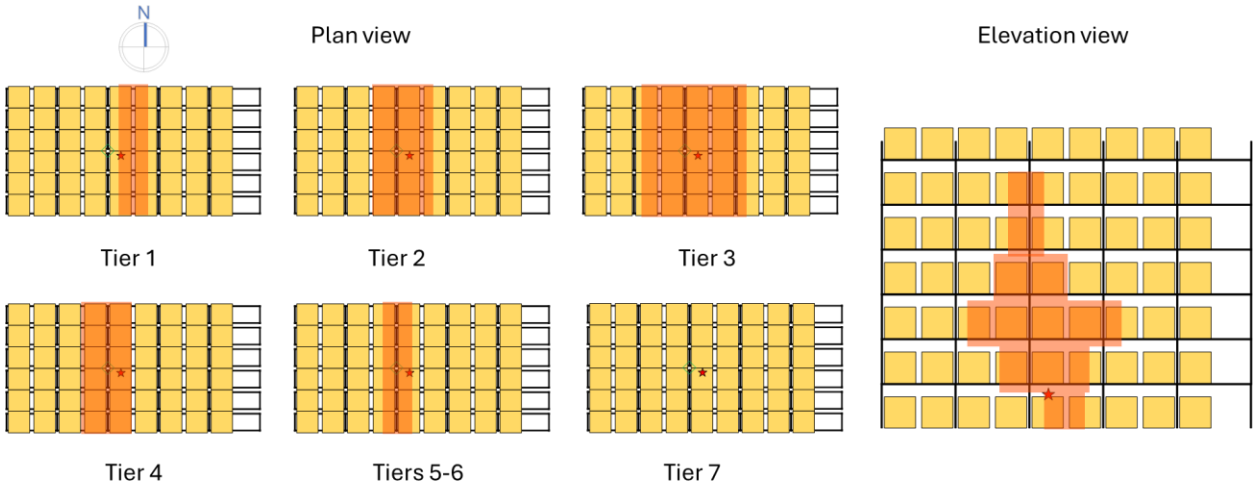

Figure 3-13: Estimated fire damage marked by orange of Test LS-1

The maximum ceiling steel temperature was about 151°C (304°F), which is lower than the failure threshold for structure damage. However, given the other results including number of sprinkler activations and extent of flame spread, the sprinkler protection would eventually be overtaxed, leading to a reduced water discharge from active sprinklers, and eventually damage to the building structure without prompt response and intervention by the local fire department. Taken together, these results indicate that the tested protection design was inadequate.

Figure 3-14 shows the sprinkler operation times and pattern of Test LS-4 where aisle spaces were doubled from Test LS-1. The first two sprinklers above the ignition location activated at 01:52 and 03:48. The third and fourth sprinklers over the south aisle activated slightly earlier than in Test LS-1, preventing the south target ignition. The sprinklers over the north aisle also activated earlier than Test LS-1, but due to skipping the sprinkler right above the target array, the fire jumped the aisle and ignited the north target. This result suggests that the tested sprinkler design is likely insufficient to control an active fire underneath but can prevent target ignition with prewetting if sprinklers activate quickly and without skipping. After the fire jumped the aisle, seven more sprinklers activated on both sides of the north aisle. Through the end of the test, the three sprinklers over the target array did not activate. The test was terminated at 09:00 due to laboratory smoke emission limits. Despite the short test duration, 15 sprinklers activated, including three at the perimeter of the ceiling, again indicating a risk of further activation should the ceiling be larger.

Figure 3-15 shows images taken at various events during Test LS-4. The top panels show views of the south aisle while the bottom panels show the north aisle. The flame spread in both directions was nearly identical, reaching the face around 02:00 and developing vertically along the face over the following two minutes to reach the top of the fifth tier. Afterward, two sprinklers activated on each side. However, the location of the activated sprinklers led to different outcomes, as discussed above. In particular, the failure to activate sprinklers over the north target resulted in the fire jumping across the aisle and a large fire burning at the faces of the main and target arrays. By comparison, the timely activation of the fourth sprinkler over the south target effectively prewetted the target array and prevented its ignition.

The extent of fire damage was similar to that in Test LS-1 and the maximum ceiling steel temperature was about 189°C (372°F), which is slightly higher than that in Test LS-1 but still much lower than the failure threshold. With similar results, the protection was again deemed as inadequate due to uncontrolled flame spread and an excessive number of sprinkler activations.

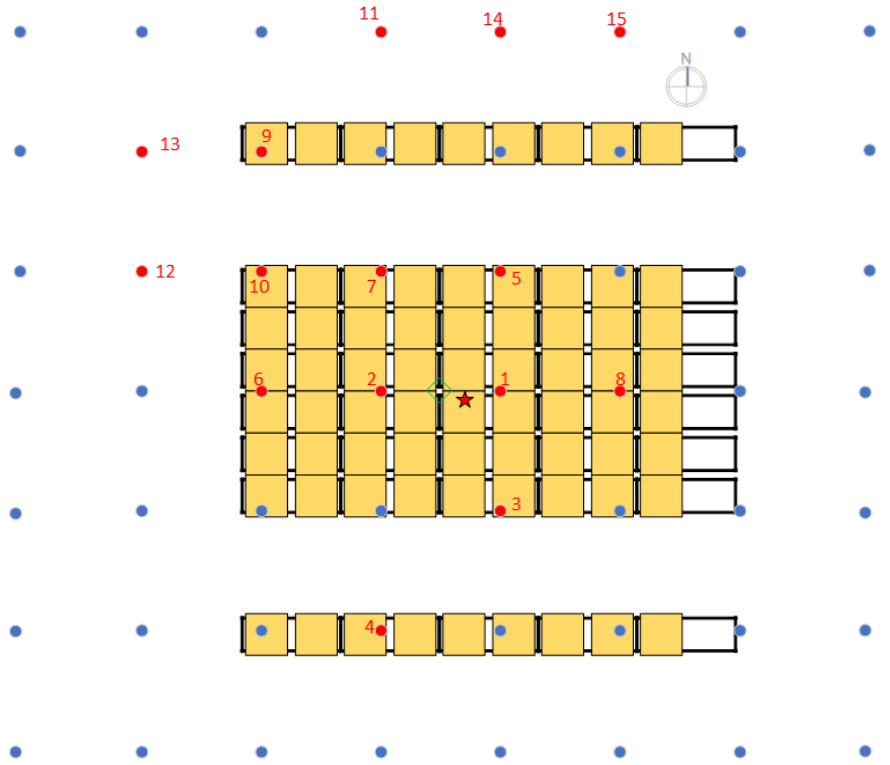

No.	Time (mm:ss)
1	1:52
2	3:48
3	4:28
4	4:29
5	4:52
6	4:53
7	5:32
8	6:39
9	6:49
10	6:51
11	7:09
12	7:39
13	7:52
14	7:52
15	8:57

Figure 3-14: Sprinkler operation times and pattern of Test LS-4

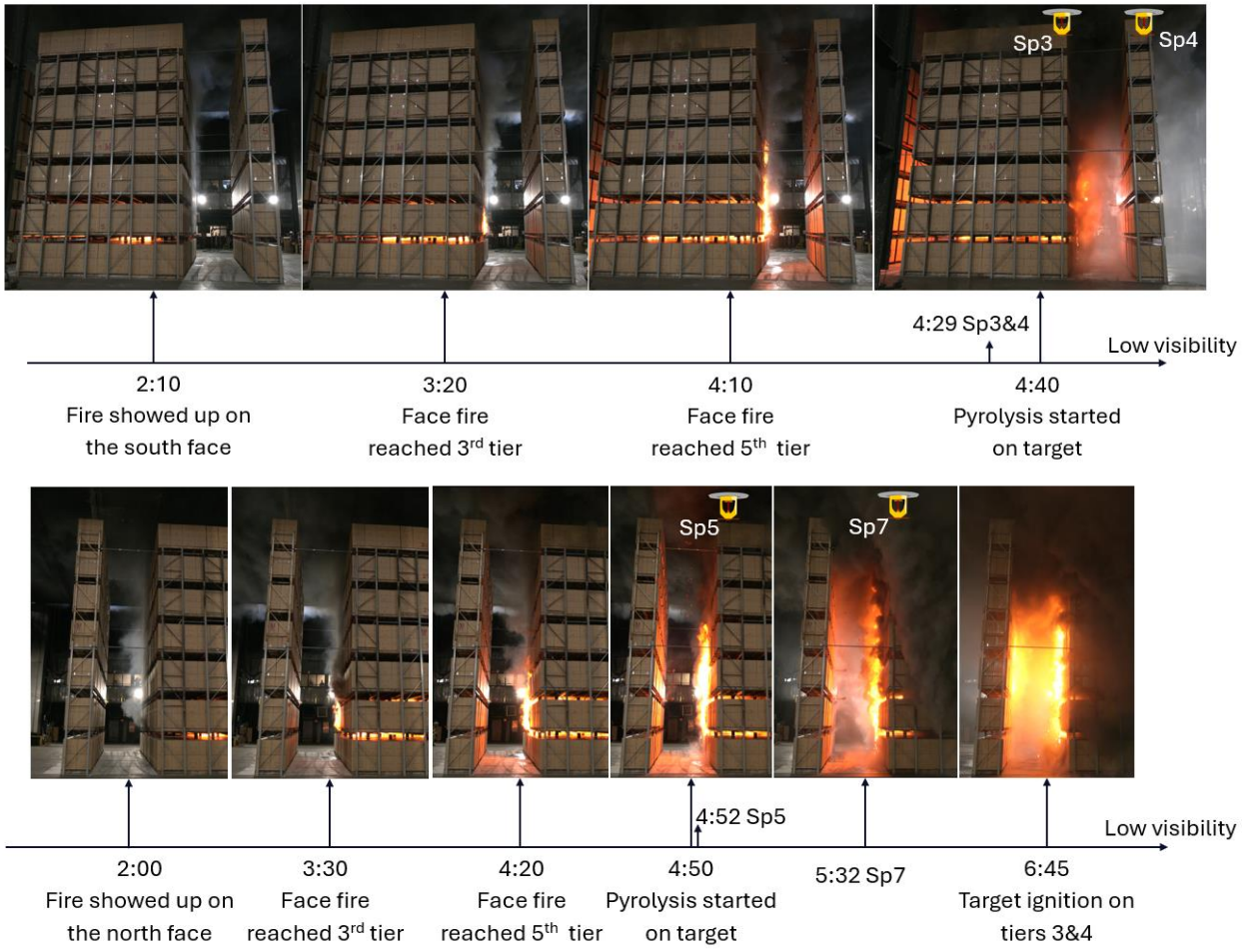

Figure 3-15: Images at various times during Test LS-4

Figure 3-16 shows the sprinkler operation times and pattern of Test LS-5 where pressure increased to 6.2 bar (90 psi) compared with Test LS-1. The first sprinkler activated around 02:38, again close to the ignition location. The second sprinkler activated around 04:47. The flame spread pattern before the second sprinkler activation was again like that in Test LS-1. However, with two sprinkler activations, the fire was controlled due to increased water pressure and discharge density. The increased water density likely speeds up downward water transport, achieving prewetting ahead of flame spread. The maximum ceiling steel temperature was about 39°C (103°F), which is well below the failure threshold.

Figure 3-17 shows images taken at various events during Test LS-5. The top panels show the views of the south aisle while the bottom panels show the north aisle. The flame spread in both directions were again almost identical, except that fire extension was observed at the south face of the main array, although without flame attachment. The fire was effectively controlled within the main array with two sprinkler activations.

Figure 3-18 shows the images taken after the test, including the manual firefighting at the north and south faces of the main array. The overall fire damage was limited and primarily contained to the area near the ignition location. However, many pallets needed to be removed to provide access for final extinguishment. The total heat release during the course of Test LS-5 was about 1,486 MJ, roughly equivalent to the total energy of one pallet load of standard CUP commodity.

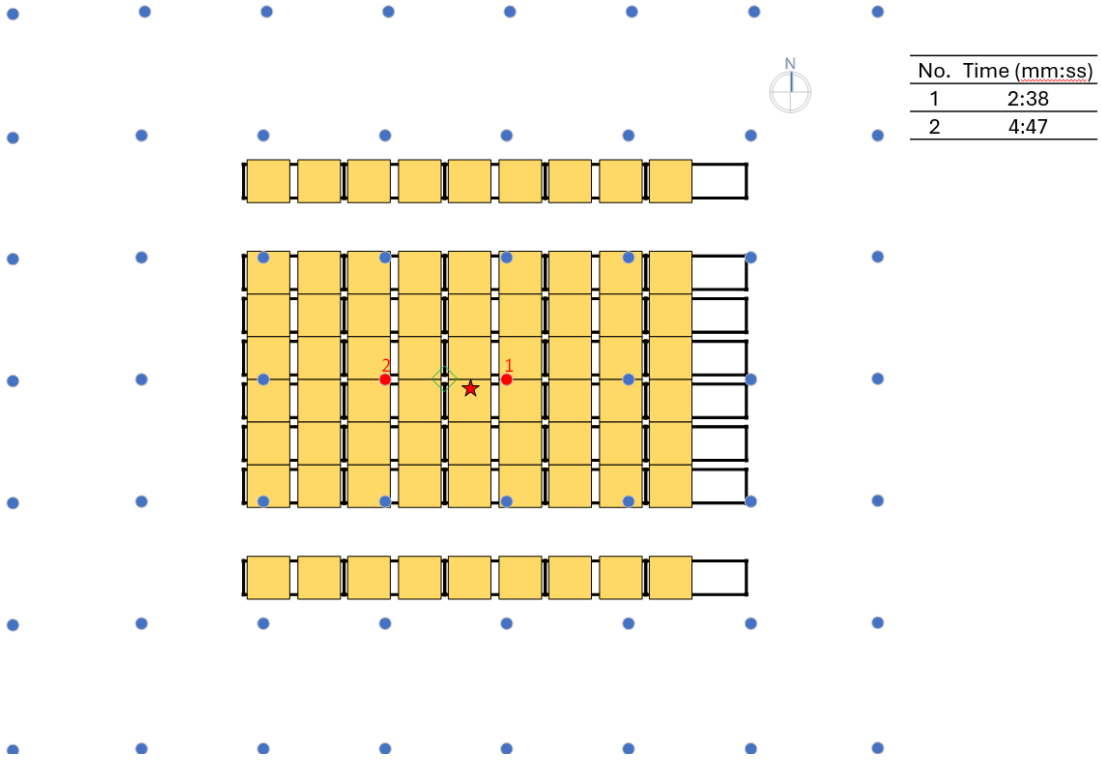

Figure 3-16: Sprinkler operation times and pattern of Test LS-5

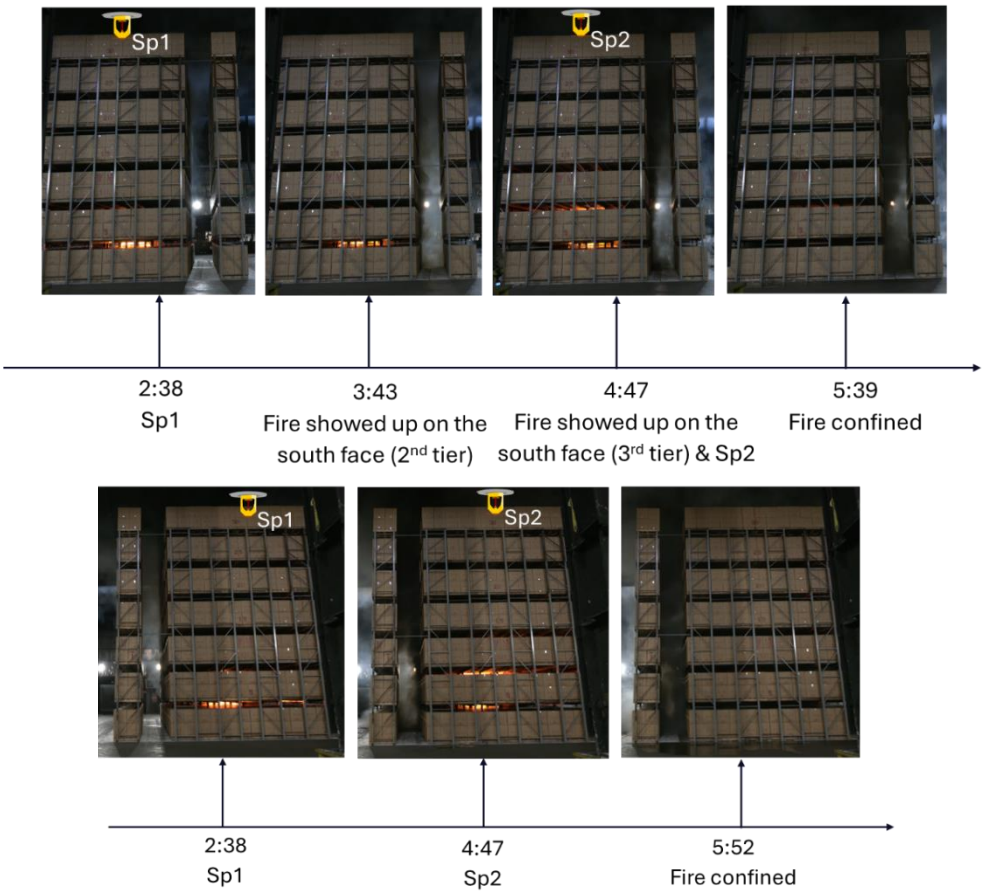

Figure 3-17: Images at various times during Test LS-5

Figure 3-18: Images taken after test for damage assessment of Test LS-5

3.3.3 Developing Protection Options for New Installations (Large-Scale Tests 2 and 3)

Figure 3-19 shows the sprinkler activation pattern of Test LS-2 where K360 lpm/bar$^{1/2}$ (K25.2 gpm/psi$^{1/2}$) sprinklers were used at 5.2 bar (75 psi), A single sprinkler activated at 02:00 before the end of the test. The fire was well confined around the ignition location, and the maximum ceiling steel temperature was about 89°C (192°F). Taken together, these results indicate that the tested protection was adequate.

Test LS-3, which reduced pressure to 2.8 bar (40 psi) had a similar result with a single sprinkler activation at 02:10. The fire was again confined to the ignition area, and the maximum ceiling steel temperature was about 85°C (185°F). The protection was also deemed adequate.

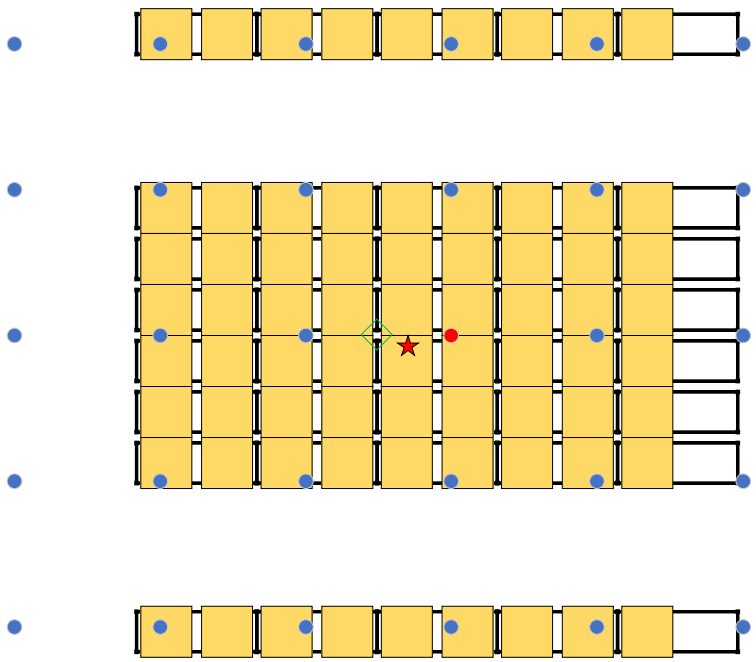

Figure 3-19: Sprinkler operation times and pattern of Test LS-2

3.3.4 Considerations on Final Extinguishment

Figure 3-20 shows the images taken during the manual firefighting process after Test LS-1. While efforts were made to document the manual firefighting process, it must be recognized that the resources and capability of the firefighting staff at the FM Research Campus may be challenging to replicate in a real warehouse fire response scenario. The manual firefighting process involved special tools such as scissor lifts for firefighters to reach upper storage areas and forklifts to dismantle the storage array and gain access to deep-seated burning areas. The time to achieve final extinguishment in these optimal conditions was still more than two hours for an uncontrolled fire scenario such as Test LS-1 and over 30 minutes for a controlled fire scenario such as Test LS-4. Those time estimates should be expected to increase for realistic fire department response conditions, depending on quality of pre-incident planning, the experience of the firefighters, and available tools. An operational plan for final extinguishment should be developed under a cooperative effort with the owners/operators, the fire service and other service providers such as restoration services, material handlers, or storage system vendors, when appropriate.

These challenges in achieving final extinguishment of MRR storage fires have an implication on the application of the test results. In Tests LS-2, LS-3, and LS-5, the fire was well confined by one or two sprinklers, which would typically suggest the adequate protection design can be applied to an unlimited storage area. However, the challenge and expected duration of manual firefighting efforts required to achieve final extinguishment, which can increase exponentially with the storage area, will demand a large water supply from the sprinkler system to cover the expected firefighting response duration. The challenges to achieving final extinguishment may also require larger water supply volumes than the typical 60-minute duration. Therefore, the practical storage area for any adequate sprinkler designs based on these test results should be limited under consideration of the locally available water supply and the capability of local firefighters to access and extinguish the fire.

Figure 3-20: Images taken during the manual firefighting process after Test LS-1

4. Conclusions and Recommendations

This work systematically evaluated the effectiveness of sprinkler fire protection strategies for multi-row rack (MRR) storage systems, focusing on both existing facilities and new installations, using both intermediate-scale and large-scale experimental tests, as well as validated numerical modeling. The key conclusions are:

1. Existing protection guidance using K240 lpm/bar$^{1/2}$ (16.8 gpm/psi$^{1/2}$) sprinklers operating at 3.6 bar (52 psi) was shown to be inadequate for closed-array MRR storage that is 10.4 m (34 ft) tall and 6.4 m (21 ft) deep under a 12.2 m (40 ft) ceiling, as evidenced by excessive sprinkler activations and uncontrolled flame spread in multiple large-scale tests. Enhanced protection using the same sprinkler but at an elevated pressure of 6.2 bar (90 psi) or, alternatively, larger K360 lpm/bar$^{1/2}$ (25.2 gpm/psi$^{1/2}$) sprinklers operating at 2.8 bar (40 psi), both demonstrated adequate fire control with one or two activations and fire containment within the main array.

2. A seamless cartoned unexpanded plastic (CUP) commodity was determined as a representative hazard for protection evaluation of MRR systems, avoiding challenges associated with differentiating commodities and monitoring or enforcing storage of specific kinds of commodities. This conclusion is based on the significant role that water transport through the seams had on lateral flame spread, which is very important for closed MRR arrays that feature long horizontal surfaces uninterrupted by flue spaces.

3. Features such as angle irons and sloped racks, which are present in different types of MRR systems, were found to have minimal impact on overall fire suppression effectiveness and do not need to be considered when evaluating protection designs for the types of multiple-row racks evaluated in this program.

4. The duration and complexity of manual fire extinguishment in large MRR storage systems should be recognized as a significant challenge, particularly for uncontrolled fire scenarios. In practical applications, the findings presented in this work should be applied with consideration of local firefighting capabilities and available water supply to define appropriate size limitations for continuous blocks of MRR storage. An operational plan for final extinguishment should be developed with input from all stakeholders such as owners and fire service. The challenges to achieving final extinguishment may require larger water supply volumes than the typical 60-minute duration. Increasing the duration of the fire protection supply should be considered.

This work also validated the use of the FireFOAM model for MRR systems. The models captured the HRR well for intermediate-scale tests, provided critical insights into worst-case ignition scenarios, and accurately predicted suppression outcomes, including the number of sprinkler activations observed in large-scale tests. Looking forward, these models can be extended to a broader range of MRR configurations, enabling reasonable interpolation or extrapolation across different ceiling heights and commodity types when ceiling-only sprinkler protection is used. This capability has the potential to reduce reliance on costly large-scale testing and accelerate project delivery. While in-rack sprinkler designs were not addressed in this effort, they remain an important consideration for retrofit applications where existing ceiling-level protection is insufficient or where storage heights exceed the range evaluated in this study.

References

[1] FM Property Loss Prevention Data Sheet 8-9, Storage of Class 1, 2, 3, 4 and Plastic Commodities, July 2025.

[2] NFPA 13, Standard for the Installation of Sprinkler Systems, 2025 Edition.

[3] Factory Mutual Research Corporation, "Rack storage fire protection committee report – Test No. 60 through 154," 1975.

[4] R. Dean, "Early suppression fast response sprinkler protection for multirow rack storage," September 1986.

[5] T. Bellamy, "Sprinkler protection for multiple-row rack storage systems - phase 1," May 2024.

[6] H. Kung, H.-Z. Yu and R. Spaulding, "Ceiling flows of growing rack storage fires," *Proceedings of the Combustion Institute,* vol. 21, pp. 121-128, 1988.

[7] Y. Xin and F. Tamanini, "Assessment of commodity classification for sprinkler protection using representative fuels," in *Fire Safety Science - Proceedings of the Ninth International Symposium*, Karlsruhe, Germany, 2008.

[8] Y. Xin, "Effects of storage height on critical delivered flux of representative fuels," *Fire Safety Journal,* vol. 91, pp. 624-632, 2017.

[9] Y. Wang, K. Meredith, X. Zhou, P. Chatterjee, Y. Xin, M. Chaos, N. Ren and S. Dorofeev, "Numerical simulation of sprinkler suppression of rack storage fires," in *Fire Safety Science - Proceedings of the Eleventh International Symposium*, Canterbury, New Zealand, 2014.

[10] N. Ren, J. de Vries, X. Zhou, M. Chaos, K. Meredith and Y. Wang, "Large-scale fire suppression modeling of corrugated cardboard boxes on wood pallets in rack-storage configurations," *Fire Safety Journal,* vol. 91, pp. 695-704, 2017.

[11] Y. Wang, P. Chatterjee and J. de Ris, "Large eddy simulation of fire plumes," *Proceedings of the Combustion Institute,* vol. 33, pp. 2473-2480, 2011.

[12] N. Ren and Y. Wang, "A convective heat transfer model for LES fire modeling," *Proceedings of the Combustion Institute,* vol. 38, pp. 4535-4542, 2021.

[13] M. Chaos, M. Khan and S. Dorofeev, "Pyrolysis of corrugated cardboard in inert and oxidative environments," *Proceedings of the Combustion Institute,* vol. 34, pp. 2583-2590, 2013.

[14] K. Meredith, J. de Vries, Y. Wang and Y. Xin, "A comprehensive model for simulating the interaction of water with solid surfaces in fire suppression environments," *Proceedings of the Combustion Institute,* vol. 36, pp. 3177-3184, 2013.

[15] G. Agarwal, A. Gupta, M. Chaos, K. Meredith and Y. Wang, "Experimental investigation and inverse modeling of the flammability behavior of cartoned plastic commodity," *Proceedings of the Combustion Institute,* vol. 36, pp. 3177-3184, 2017.

[16] Y. Wang and M. Chaos, "CFD modeling of flame spread over corrugated cardboard panels," in *Fire and Materials 2013 - 13th International Conference and Exhibition*, San Francisco, USA, 2013.

[17] S. Dorofeev, "Thermal quenching of mixed eddies in non-premixed flames," *Proceedings of the Combustion Institute,* vol. 36, pp. 2947-2954, 2017.

[18] N. Ren, D. Zeng, K. Meredith, Y. Wang and S. Dorofeev, "Modeling of fame extinction/re-ignition in oxygen-reduced environments," *Proceedings of the Combustion Institute,* vol. 37, pp. 3915-3958, 2019.

[19] D. Han, "A machine learning based approach to model sprinkler actual delivered density, part 1: ignition under 1 sprinkler," FM, April 2025.

[20] D. Han, S. Chen, Y. Gopala, S. Sienkiewicz, B. Ditch and Y. Xin, "A machine learning-based approach to model sprinkler actual delivered density," in *Proceedings of the Eleventh International Seminar on Fire and Explosion Hazards (ISFEH 11)*, Rome, Italy, 2025.

[21] FM Property Loss Prevention Data Sheet 2-0, Installation Guidelines for Automatic Sprinklers, April 2025.

FM

InsurerFM

FMGlobal

TheFMGroup